

Heating of Galactic Disks by Infalling Satellites

A. J. Benson^{1,3}, C. G. Lacey², C. S. Frenk², C. M. Baugh² & S. Cole²

1. *California Institute of Technology, MC 105-24, Pasadena, CA 91125, U.S.A.*

2. *Physics Department, University of Durham, Durham, DH1 3LE, England*

3. *Current address: University of Oxford, Keble Road, Oxford, OX1 3RH (e-mail: abenson@astro.ox.ac.uk)*

4 October 2018

ABSTRACT

We develop an analytic model to calculate the rate at which galaxy disks are heated by dark matter substructures orbiting in their halos. The model takes into account the internal structure, mass function and accretion rate of satellites expected in the Λ CDM cosmology, as well as the growth of the disk by accretion and mergers, but it ignores resonant heating of the disk and the dynamical effects of spiral arms and bars. We calibrate this model against N-body simulations and demonstrate that it is able to reproduce the N-body heating rates to within a factor of 3 in the majority of cases. Our model gives the distribution of disk scale-heights for galaxies of different luminosities. For L_* spiral galaxies, it predicts a median disk thickness of only 5% of the radial scale-length if substructure is the only source of heating. The median disk thickness increases to nearly 20% of the radial scale-length when heating due to gravitational scattering of stars by molecular clouds is also included. The latter value is close to the thickness estimated observationally for the disk of the Milky Way galaxy. The distribution of disk thickness predicted by the model is also consistent with a recent observational determination for sub- L_* galaxies by Bizyaev & Mitronova (2002). Thus, the observed thickness of the stellar disks of spiral galaxies seems to be entirely compatible with the abundance of substructure in dark matter halos predicted by the standard Λ -dominated cold dark matter model of structure formation. In an $\Omega_0 = 1$ universe, our best model of galaxy formation produces similar scale-heights, a consequence of the fact that similar amounts of substructure are accreted by halos during the lifetime of the disk in $\Omega_0 = 1$ and $\Omega_0 = 0.3$, $\Lambda_0 = 0.7$ cold dark matter cosmologies.

1 INTRODUCTION

A generic prediction of hierarchical models of structure formation, such as the cold dark matter (CDM) model, is that the dark matter halos of galaxies and clusters should contain large amounts of substructure, in the form of small, gravitationally bound subhalos orbiting within the larger potential. This substructure arises because large halos are built up by mergers of smaller halos whose tidally-stripped remnants can survive in favourable conditions. Recently, it has been claimed that the CDM model predicts an order of magnitude too many subhalos around the Milky Way galaxy, compared to what is inferred from the number of satellite galaxies (Klypin et al. 1999; Moore et al. 1999). Several authors have now pointed out that this apparent discrepancy is readily explained if some process (such as the heating of the intergalactic medium (IGM) during reionization) is efficient at suppressing the formation of galaxies in most of these subhalos (Bullock, Kravtsov & Weinberg 2000; Benson et al. 2002b; Somerville 2002). In this picture, galaxy halos should be filled with many small subhalos containing neg-

ligible amounts of luminous material. A strong test of this idea is possible by searching for gravitational signatures of subhalos, thus bypassing the problem of relating subhalos to the visible material in satellite galaxies.

The most direct probe of substructure in dark matter halos is gravitational microlensing. Its properties are reasonably well understood theoretically (Mao & Schneider 1998; Metcalf & Madau 2001; Chiba 2002; Dalal & Kochanek 2002a; Dalal & Kochanek 2002b). Although the interpretation of the current datasets remains controversial in some cases, the observed microlensing rates appear to be consistent with the abundance of substructure predicted by CDM.

An alternative constraint on the amount of substructure in halos may be obtained by considering the thickness of the stellar disks of galaxies. Subhalos on orbits that pass through or near to a galactic disk perturb it gravitationally and deposit energy into it, gradually heating the disk and increasing its scale-height. Since there are other mechanisms that also heat stellar disks (but with uncertain efficiency), the observed thickness of galactic disks sets an upper limit on the abundance of such substructure. The heating of galac-

tic disks by infalling satellites was invoked as a constraint on models of structure formation by Tóth & Ostriker (1992; hereafter TO). They calculated this effect semi-analytically, and concluded that the thinness of the Milky Way’s disk is inconsistent with the hierarchical build-up of galaxies in a high density ($\Omega_0 = 1$) CDM universe. This conclusion was disputed by Navarro, Frenk & White (1994) whose cosmological simulations showed that many of the satellites that are incorporated into a galactic dark halo do not actually merge with the central galaxy. Subsequent numerical simulations of mergers of single satellites with larger disk galaxies (e.g. Huang & Carlberg 1997; Velázquez & White 1999) indicated that TO’s analytical estimates of the heating rate were somewhat too high, weakening their constraint on structure formation models. More recently, Font et al. (2001) have numerically simulated the heating of disks by the ensemble of subhalos predicted to exist within dark halos in the CDM model. Their simulations of Milky Way-like galaxies only set an upper limit to the rate of disk heating by satellites, because of numerical effects, but they conclude that this is less than the total disk heating rate that is inferred observationally for the Solar neighbourhood. They argue that the heating rates are low because the most massive satellites, which are the ones that cause the most heating, are few in number and because few satellites penetrate the inner regions of the disk. Although their conclusions agree with those of Navarro, Frenk & White (1994), they are limited by the fact that they simulated only two realizations of the halo substructure.

In this paper, we develop a new semi-analytical model of disk heating by halo substructure. Our calculation builds upon earlier semi-analytical modeling of galaxy formation within the framework of CDM cosmology (Cole et al. 2000), and on recently developed analytical models of the evolution of satellites within dark matter halos (Taylor & Babul 2001; Benson et al. 2002a; Taffoni et al. 2003; Taylor & Babul 2003). The rate at which satellite halos of different masses are incorporated into the main halo is given by the galaxy formation model. The satellite model then predicts how the masses, radii and orbits of subhalos evolve due to dynamical friction and tidal stripping by the halo, disk and bulge of the host galaxy. In this paper, we add a calculation of how much of the orbital energy of the satellites that is lost by dynamical friction goes into increasing the thickness and vertical motions of the galactic disk. The interaction between the satellite and the disk is modeled in a simplified way, ignoring details such as resonant interactions and the possible role of spiral features and bars. We test and calibrate our analytical model of satellite evolution against a new set of high-resolution N-body simulations of single satellites merging with disk galaxies. We find (as has also been shown by Taylor & Babul 2001 and Taffoni et al. 2003) that such an analytical model is able to reproduce well the behaviour seen in the N-body simulations. We measure the disk heating in the same simulations, and find that it is quite well reproduced by our analytical model. We then apply this model of heating by satellites within the framework of our semi-analytical model of galaxy formation, in order to predict

the distribution of scale-heights for disk galaxies of different luminosities.

Both the N-body and semi-analytical approaches have advantages and disadvantages when applied to this problem. N-body simulations fully account for the non-linear interaction of substructure and disk (e.g. for the excitation of global modes such as warps and bars in the disk). However, they are limited by resolution and artificial numerical heating and, because of computational cost, they are limited to few (two, in the case of the best cosmological simulations of disk heating to date, by Font et al.). The semi-analytical approach has the advantage that it is not limited by resolution or artificial heating, and it allows the calculation of a large number of realizations. Since heating by substructure is a highly stochastic process, it is important to account for the galaxy-to-galaxy variation in the heating rate by calculating a large number of realizations. At present, this is only possible with the semi-analytical approach.

The remainder of this paper is arranged as follows. In §2 we describe our analytical model for disk heating by subhalos and for the evolution of the disk scale-height. In §3 we calibrate and test our analytical model against numerical simulations of single satellite-disk mergers. In §4 we present our predictions for the distribution of scale-heights of disk galaxies in the CDM model, and compare with observational data for the Milky Way and for other galaxies. Finally, in §5 we present our conclusions. Appendices detail derivations of various formulae related to dynamical friction and disk energies and present convergence tests for the N-body simulations.

2 MODEL

2.1 Evolution of Satellites and their Orbits

We calculate the evolution of the masses, radii and orbits of satellites using a development of the model presented in Benson et al. (2002a; hereafter Paper I). That work, in turn, was based on the satellite evolution model of Taylor & Babul (2001). We summarize here the main features of our model. The growth of the main halo is described by a merger history tree which is calculated by a Monte Carlo method (Cole et al. 2000). When smaller halos (in general containing one or more visible galaxies) merge with the main halo, they become satellite halos. The satellite halos are given initial orbits which start close to the virial radius but have a range of eccentricities consistent with the distribution seen in the N-body simulations of Ghigna et al. (1998.). The satellite orbits are followed in the potential of the host system; they evolve due to dynamical friction against the dark halo, disk and bulge of the main galaxy. At the same time, the satellites lose mass by tidal stripping, both “static” tidal limitation and tidal shocking. As a satellite is tidally stripped, its radius and internal structure also change.

We have made a few improvements to our satellite orbit model from that presented in Paper I. These are described in Appendix A.

2.2 Disk Heating

2.2.1 Rate of Heating

We now wish to calculate the rate at which a satellite halo heats the disk of the galaxy in its host halo. The satellite experiences dynamical friction against the disk, and the energy lost from the orbital motion of the satellite by this mechanism goes into increasing the energy of the disk. Working in the frame in which the centre of mass of the central galaxy and its halo are at rest, the satellite injects energy into the disk at a rate

$$P = -\mathbf{F}_{\text{df,disk}} \cdot \mathbf{v}_{\text{sat}}, \quad (1)$$

where $\mathbf{F}_{\text{df,disk}}$ is the dynamical friction force exerted by the disk and \mathbf{v}_{sat} is the velocity of satellite. (Note that while we typically expect the satellite to lose energy to the disk, it is possible for the satellite to gain energy from the ordered motions of the disk if $\mathbf{F}_{\text{df,disk}} \cdot \mathbf{v}_{\text{sat}} > 0$. This occurs because the dynamical friction force depends, in our approximation, on the relative velocity vector of the satellite and the local disk stars. If the local disk velocity is sufficiently large, the relative velocity vector may point in the opposite direction to the satellite velocity vector, resulting in a transfer of energy from the disk to the satellite.) This energy is initially injected in the form of kinetic energy, but it is subsequently mixed between kinetic and potential energies by the motions of the stars. We are interested in the increase in the vertical energy of the disk, which is given by

$$\dot{E}_z = -\epsilon_z \mathbf{F}_{\text{df,disk}} \cdot \mathbf{v}_{\text{sat}}, \quad (2)$$

We derive an expression for the efficiency factor $\epsilon_z \leq 1$ in Appendix B3 by considering the increases in the vertical and horizontal components of the velocity dispersion of the stars responsible for dynamical friction during scattering events. This expression (B29) depends only on the Coulomb logarithm, $\ln \Lambda$, and the angle θ_{V_0} between the disk-satellite relative velocity and the z -axis. We then simply integrate \dot{E}_z along the satellite orbit to determine the net increase in the disk's vertical energy.

Figure 1 shows how ϵ_z depends on the angle θ_{V_0} for a few representative values of Λ . Note that $\epsilon_z = \frac{1}{3}$ when $\cos \theta_{V_0} = \frac{1}{\sqrt{3}}$, independently of Λ . For small Λ the efficiency is greatest when $\theta_{V_0} = 0^\circ$ (approaching unity as Λ approaches zero) and smallest for $\theta_{V_0} = 90^\circ$ (approaching zero as Λ approaches zero). For large Λ the trend is reversed, with ϵ_z being smallest at $\theta_{V_0} = 0^\circ$ (approaching zero as Λ approaches infinity) and largest for $\theta_{V_0} = 90^\circ$ (approaching $\frac{1}{2}$ as Λ approaches infinity). The transition between these two regimes occurs for $\Lambda \approx 3.975$, for which ϵ_z is independent of θ_{V_0} .

We can understand the behaviour of ϵ_z in simple terms. For example, for $\theta_{V_0} = 0$, the efficiency drops to zero as Λ becomes large. In this case, vertical motions in the disk are parallel to the relative velocity vector of the satellite and the disk stars. Consequently, only the $\Delta V_{\text{m}\parallel}$ term (see eqn. B15) contributes to increasing the energy in these vertical motions. As Λ , and hence the maximum impact parameter, b , increases, energy transfer from the satellite becomes dominated by large b scatterings. For large impact param-

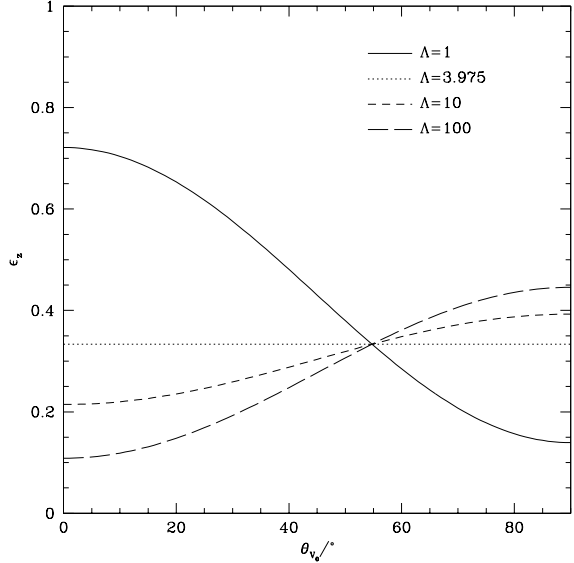


Figure 1. The efficiency of energy transfer to vertical motions in the disk as a function of the angle between the disk-satellite relative velocity and the z -axis, θ_{V_0} . Results are plotted for several values of Λ as indicated in the figure.

eters, the increase in velocities (and hence energies) perpendicular to the satellite motion dominates over that parallel to the motion, since $\Delta V_{\text{m}\parallel} \propto b^{-2}$ while $\Delta V_{\text{m}\perp} \propto b^{-1}$ (see eqn. B16). Consequently, the efficiency of transfer to vertical motions in the disk drops to zero as Λ becomes large.

The reversal of the trend of ϵ_z with θ_{V_0} at $\Lambda \approx 3.975$ is also simple to understand. For larger Λ , energy transfer is predominantly into motions perpendicular to the motion of the satellite (as discussed above). Thus, the efficiency of energy transfer to motions in the vertical direction is greatest when the satellite moves perpendicular to that direction ($\theta_{V_0} = 90^\circ$). For smaller Λ , energy transfer occurs mostly into the parallel direction, and so ϵ_z is maximized for $\theta_{V_0} = 0^\circ$. For $\Lambda \approx 3.975$ energy transfers into perpendicular and parallel directions are equal and so ϵ_z is constant.

When $\cos \theta_{V_0} = \frac{1}{\sqrt{3}}$, the energy transferred to vertical motions is always one third of the increase in energy parallel to the satellite velocity, plus one third of the increase in the energies in the two directions perpendicular to the satellite velocity. Thus, this energy is always exactly one third of the total energy transferred from the satellite and hence $\epsilon_z = \frac{1}{3}$ independently of Λ .

It is worth considering at this point some of the simplifications which go into our dynamical model of disk heating. Dynamical friction is treated using Chandrasekhar's approximation which is clearly not strictly applicable to our halo-plus-disk system. While this approximation has been shown to be a reasonable one for dark matter halos (Weinberg 1986; Bontekoe & van Albada 1987; Core, Muzzio & Vergne 1997; van den Bosch 1999; Velázquez & White 1999; Colpi, Mayer & Governato 1999), its validity when disks are included is less clear. Importantly, this approxima-

Table 1. Properties of the galaxy and satellite models used in the N-body simulations. The first column specifies the component in question. The second column gives the density profile, either in spherical coordinates (r), or cylindrical polar coordinates (R, z). The values of the parameters of each profile are listed in column 3. The satellites are all described by King models (King 1966). For these, we specify the core radius, r_c , and the concentration $c = \log_{10} r_t/r_c$ where r_t is the tidal radius of the satellite. The final column lists the number of particles used to represent each component in the standard case.

Component	Density Profile	Parameters	Number of Particles
Halo	$\rho_h(r) = \frac{M_h \alpha}{2\pi^{3/2} r_{\text{cut}}} \frac{\exp(-r^2/r_{\text{cut}}^2)}{r^2 + \gamma^2}$	$M_h = 7.84 \times 10^{11} M_\odot$ $\gamma = 3.5 \text{ kpc}$ $r_{\text{cut}} = 84 \text{ kpc}$ $\alpha = 1.076$	687008
Disk	$\rho_d(R, z) = \frac{M_d}{4\pi R_d^2 H_d} \exp(-R/R_d) \text{sech}^2(z/H_d)$	$M_d = 5.6 \times 10^{10} M_\odot$ $R_d = 3.5 \text{ kpc}$ $H_d = 700 \text{ pc}$	163840
Bulge	$\rho_b(r) = \frac{M_b}{2\pi} \frac{a}{r(a+r)^3}$	$M_b = 1.87 \times 10^{10} M_\odot$ $a = 525 \text{ pc}$	16384
Satellite S1	King Model	$M_s = 5.60 \times 10^9 M_\odot$ $r_c = 1 \text{ kpc}$ $c = 0.8$	32768
Satellite S2	King Model	$M_s = 5.60 \times 10^9 M_\odot$ $r_c = 500 \text{ pc}$ $c = 1.1$	32768
Satellite S3	King Model	$M_s = 1.12 \times 10^{10} M_\odot$ $r_c = 875 \text{ pc}$ $c = 1.0$	32768

Table 2. Properties and initial orbital parameters of the satellites in the N-body simulations. Column 2 specifies the satellite model used (as defined in Table 1). Column 3 lists θ_i , the angle between the initial angular momentum vector of the satellite and that of the disk. Column 4 lists the circularity of the satellite's initial orbit, ϵ_J , while column 5 lists the initial radial position of the satellite (which is the apocentre of its orbit), r_a . Column 6 specifies whether the simulation contains a disk or not (note that θ_i is undefined for diskless simulations G2Sxx).

Model	Satellite	θ_i	ϵ_J	r_a/kpc	Disk?
G1S1	S1	45°	0.33	59.0	✓
G1S2	S1	0°	0.55	55.0	✓
G1S3	S1	45°	0.55	55.0	✓
G1S4	S1	90°	0.55	55.0	✓
G1S5	S1	135°	0.55	55.0	✓
G1S6	S1	180°	0.55	55.0	✓
G1S7	S1	0°	0.82	46.5	✓
G1S8	S1	45°	0.82	46.5	✓
G1S9	S2	0°	0.55	55.0	✓
G1S10	S2	45°	0.55	55.0	✓
G1S11	S2	90°	0.55	55.0	✓
G1S12	S2	135°	0.55	55.0	✓
G1S13	S2	180°	0.55	55.0	✓
G1S14	S3	45°	0.55	55.0	✓
G1S15	S3	135°	0.55	55.0	✓
G2S1	S1	N/A	0.33	59.0	×
G2S2	S1	N/A	0.55	55.0	×
G2S7	S1	N/A	0.82	46.5	×
G2S9	S2	N/A	0.55	55.0	×
G2S14	S3	N/A	0.55	55.0	×

tion ignores any possible resonant interaction between the satellite and the disk.

A further simplification of our model is that the phase space distributions of halo dark matter and disk stars are assumed to be fixed, with the exception that the disk vertical velocity dispersion and density profile are allowed to change with time. (We further assume that the vertical motions of stars in the disk do not couple to radial and azimuthal motions, which will be approximately true provided that the disk remains thin.) In reality, all three components of the disk velocity dispersion will be affected by substructure heating. However, the changes in the radial and azimuthal velocity dispersions have only a small effect on the overall structure of the disk in the majority of cases. Thus, our approach should be a reasonable first approximation.

A final, important simplification is that we ignore some possible interactions between the disk and the dark matter halo, e.g. those driven by non-axisymmetric structures such as bars or warps in the disk. This complex set of interactions could, in principle, result in energy initially transferred from the satellite to the disk finding its way into the halo dark matter. The efficiency with which this happens will clearly depend upon the frequency with which substructure excites bars and other global modes in the disk and is therefore beyond the scope of our current calculations.

Given these simplifications it is important to test our analytic calculations against N-body simulations of the disk heating process. We perform such tests in §3.

Table 3. Comparison of results from the analytic and N-body calculations of satellite evolution. Column 1 lists the model number; column 2 lists the type of calculation (analytic or N-body); column 3 gives the change in the disk vertical kinetic energy generated by the satellite at the end of the simulation, both in absolute units and as a percentage of the initial disk vertical kinetic energy (values in parentheses). Where the analytic and N-body estimates of the disk energy differ by more than a factor of two, we show the values in bold type. Columns 4 and 5 list the times at which the satellite reaches 50% and 10% of its initial mass respectively.

Model	Type	$\frac{\Delta T_z(4\text{Gyr})}{10^{14} M_\odot \text{km}^2 \text{s}^{-2}}$	t_{50}/Gyr	t_{10}/Gyr
G1S1	Analytic	0.133 (25%)	1.24	2.01
G1S1	N-body	0.101 (18%)	1.38	2.16
G1S2	Analytic	0.257 (49%)	1.51	2.89
G1S2	N-body	0.342 (60%)	1.69	2.08
G1S3	Analytic	0.184 (35%)	2.20	3.19
G1S3	N-body	0.238 (42%)	2.25	3.13
G1S4	Analytic	0.029 (5%)	2.32	3.73
G1S4	N-body	0.101 (18%)	2.54	3.53
G1S5	Analytic	0.032 (6%)	2.24	3.77
G1S5	N-body	0.057 (10%)	2.46	3.55
G1S6	Analytic	0.177 (33%)	1.94	3.00
G1S6	N-body	0.090 (16%)	2.21	3.14
G1S7	Analytic	0.056 (11%)	2.70	> 4.00
G1S7	N-body	0.443 (77%)	2.22	2.28
G1S8	Analytic	0.096 (18%)	3.23	> 4.00
G1S8	N-body	0.324 (57%)	3.72	4.03
G1S9	Analytic	0.272 (51%)	1.92	3.30
G1S9	N-body	0.307 (54%)	1.82	1.88
G1S10	Analytic	0.244 (46%)	2.53	3.28
G1S10	N-body	0.588 (103%)	3.01	3.35
G1S11	Analytic	0.114 (22%)	2.86	3.59
G1S11	N-body	0.363 (63%)	3.16	3.80
G1S12	Analytic	0.131 (25%)	2.89	3.58
G1S12	N-body	0.229 (40%)	3.26	4.06
G1S13	Analytic	0.507 (96%)	2.32	2.62
G1S13	N-body	0.350 (61%)	2.87	3.28
G1S14	Analytic	0.521 (98%)	1.58	2.52
G1S14	N-body	0.873 (153%)	1.62	1.90
G1S15	Analytic	0.438 (83%)	1.78	2.09
G1S15	N-body	0.374 (65%)	1.80	2.18

2.2.2 Disk Scale-Height and Vertical Energy

Having calculated the energy deposited into vertical motions of disk stars, we now wish to calculate the resulting scale-height of the disk. We work throughout in the *thin disk approximation*, in which the vertical extent of the disk is always assumed to be small compared to its radial extent, and the

non-circular velocities are assumed to be small compared to the circular velocity. In this approximation, the disk can be treated as being locally plane-parallel, with the consequence that the vertical motions separate from the motions in the plane, and there is a well-defined vertical energy which (in the absence of perturbations by satellites or other objects) is conserved both for individual stars and for the disk as a whole. The vertical energy given to a star by an encounter with a satellite is initially in the form of vertical kinetic energy, but the orbital motion of the star subsequently mixes this between vertical kinetic and potential energies, while keeping the sum of the kinetic and potential energies constant. In the thin disk approximation, the total vertical energy per unit area of the disk, e_z , can be written as (TO)

$$e_z = t_z + w_{\text{dd}} + w_{\text{dh}}, \quad (3)$$

where all quantities are surface energy densities, t_z is the disk vertical kinetic energy, w_{dd} is the disk self-gravitational energy and w_{dh} is the gravitational energy due to the disk/halo interaction. The vertical energy e_z is defined to be zero in a state where the disk has zero thickness and zero vertical velocities. Expressions for t_z , w_{dd} and w_{dh} are derived in Appendix C. Following TO, we assume virial equilibrium and find

$$2t_z - w_{\text{dd}} - 2w_{\text{dh}} = 0, \quad (4)$$

and so

$$e_z = \frac{3}{2}w_{\text{dd}} + 2w_{\text{dh}}. \quad (5)$$

The density of our model disks in the vertical direction is proportional to $\text{sech}^2 z/H_d$. For this density profile we find from eqn.(5) (TO)

$$e_z = \frac{3}{2}\pi G \Sigma_d^2(R) H_d + \frac{\pi^2}{12} \Sigma_d(R) H_d^2 \frac{GM_h(R)}{R^3}, \quad (6)$$

where R is radius in the disk plane, $\Sigma_d(R)$ is the disk surface mass density, and $M_h(R)$ is the mass in the (spherical) halo plus bulge within radius R . Since the vertical kinetic energy per unit area is $t_z = \frac{1}{2}\Sigma_d \sigma_z^2$, we also find from eqn.(4)

$$\sigma_z^2 = \pi G \Sigma_d(R) H_d + \frac{\pi^2}{12} GM_h(R) H_d^2 / R^3 \quad (7)$$

This expression is used to calculate the vertical velocity dispersion at each radius from the scale-height H_d . *

To relate the radially-dependent vertical energy per unit area to the global total vertical energy, we make the assumption that the disk scale-height is constant with radius, since this is observed to be a good approximation for real galaxies (e.g. de Grijs & Peletier 1997). We can then integrate eqn.(6) over the whole disk to find the total vertical energy. Using $\Sigma_d = (M_d/2\pi R_d^2) \exp(-R/R_d)$ for an exponential disk of radial scale-length R_d we find

$$E_z = \frac{3}{16} M_d V_d^2 h + \frac{\pi^2}{12} M_d V_d^2 h^2 \int_0^\infty \left[\frac{V_h}{V_d} \right]^2 \frac{\exp(-x)}{x} dx, \quad (8)$$

* Note that here we differ slightly from VW by including the contribution of the halo gravity to the disk vertical velocity dispersion. This is typically a small, although not negligible, contribution over the bulk of the disk.

where the fractional scale-height $h = H_d/R_d$, $V_d^2 = GM_d/R_d$ and $V_h^2 = GM_h(R)/R$. Integrating eqn.(7) gives a similar expression for the total vertical kinetic energy T_z . Once the total vertical energy E_z is known, the above equation is easily solved for h and hence H_d .

2.2.3 Local vs. Global Heating

In §2.2.2 we made the assumption that the energy deposited in the disk by satellites was distributed throughout the disk in such a way as to produce a scale-height that was independent of radius. However, the increase in energy per unit mass caused by a satellite passing through or near the disk will initially be greatest close to the point of impact. Since satellite encounters frequently trigger global modes of the disk it is not implausible that this energy quickly becomes redistributed throughout the disk. However, it is interesting to consider the opposite extreme in which energy is deposited at the position of the satellite and remains there. We refer to these two extremes as “global” and “local” heating. To study local heating we accumulate the energy deposited by satellites in a narrow annulus of the disk (in practice we use a Gaussian window function), centred on the disk half-mass radius. We then assume that the specific energy of disk material is proportional to the same window function and use the relations of §2.2.2 to compute the resulting scale-height at the half-mass radius.

Observations of real galactic disks (de Grijs & Peletier 1997) indicate that the scale-height is reasonably constant with radius, at least for late-type galaxies. For this reason we prefer the global heating assumption, but consider local heating also as an interesting comparison.

2.2.4 Further Aspects

Below we detail how we deal with energy[†] deposited in a gaseous disk and how we treat galaxy mergers, gas accretion and star formation.

Gas in Galaxy Disks: Disks in our model in general consist of both stars and gas. The gas is assumed to be in an infinitely thin layer with zero velocity dispersion in the disk midplane. We include the contribution of the gas to the disk gravitational potential and when computing the disk scale-height. With our choice of zero-points for the energy, the vertical kinetic energy of the gas and also its self-gravitational energy are both zero (because it is at $z = 0$), but the gas contributes to the total energy per unit area of the disk e_z through the gravitational interaction energy between the gas and stars (see TO for more details). We assume that gas and stars in the disk are heated at the same rate per unit mass, but that the gas dissipates this energy rapidly, so that energy deposited in the gas is effectively lost.

Adiabatic Heating due to Gas Accretion: Gas accreted

onto the disk is assumed to initially have zero energy. However, the growth of the disk surface density causes gravitational compression in the vertical direction, which tends to increase the vertical energies of disk stars. We follow TO and assume that gas infall occurs adiabatically, adopting their equation (3.12) to describe the change in energy of the disk stars due to adiabatic heating. In our model, gas can also be lost from the disk due to feedback processes, resulting in a decrease in the energies of stars. We account for this process in the same way as for the adiabatic heating, simply changing the sign of the effect. We find that these are minor effects that have little impact on the predicted scale-heights of disk galaxies.

Star Formation: When gas turns into stars, we assume that these stars start out with zero energy, but then rapidly mix with the pre-existing stellar population, conserving the total disk vertical energy.

Galaxy Mergers: In a major merger all disks are destroyed, and so we zero the energy of the resulting galaxy. In minor mergers, stars from the satellite galaxy disk and bulge are added to the bulge of the central galaxy. In the merger, the energy of the satellite disk is lost, while that of the central galaxy disk is unchanged, unless the infalling satellite contains gaseous material, which will contribute to the adiabatic heating of the central galaxy disk.

2.2.5 Heating of Disks by Scattering by Clouds

Substructure in the halo is not the only source of heating for disks. Two other plausible mechanisms for disk heating are gravitational scattering of stars by massive gas clouds (Spitzer & Schwarzschild 1953; Lacey 1984) and scattering of stars by spiral arms (Carlberg & Sellwood 1985). The latter mechanism is inefficient at producing any heating in the vertical direction, so we will focus on the first mechanism. Lacey (1984) derived analytical expressions for the rate at which scattering by clouds increases the vertical and horizontal epicyclic energies of the stars. In general, these expressions depend on the radial and vertical disk velocity dispersions, σ_R and σ_z , but, acting by themselves, the clouds tend to drive the ratio σ_z/σ_R to an equilibrium value. We calculate the rate of increase of vertical energy per unit mass for the stars, ε_z , using Lacey’s eqn.(39), evaluated for the equilibrium σ_z/σ_R and in the limit in which the scale-height of the stars is larger than that of the clouds. This gives

$$\left(\frac{d\varepsilon_z}{dt}\right)_{\text{clouds}} = \frac{2G^2\Sigma_c M_c \ln \Lambda_c \nu}{\sigma_z^2} \alpha_s^3(\beta) K_s(\beta) \quad (9)$$

where Σ_c is the surface density in clouds, M_c is the cloud mass, $\ln \Lambda_c$ is the Coulomb logarithm for scattering of stars by clouds and ν is the vertical epicyclic frequency. $\alpha_s(\beta)$ and $K_s(\beta)$ are functions of $\beta = 2\Omega/\kappa$ which are tabulated by Lacey, Ω being the angular velocity for circular orbits and κ the radial epicyclic frequency. We obtain the total contribution of scattering by clouds to the increase of vertical energy by integrating eqn.(9) over radius:

$$\dot{E}_{z,\text{clouds}} = \int_0^\infty \Sigma_d \left(\frac{d\varepsilon_z}{dt}\right)_{\text{clouds}} 2\pi R dR \quad (10)$$

[†] For convenience, we use the expression “energy” to imply “disk vertical energy” from here on, unless explicitly stated otherwise.

Numerical simulations of heating by clouds agree fairly well with the velocity dependence predicted analytically, ($d\sigma^2/dt \propto \sigma^{-2}$), but have given somewhat conflicting results about the amplitude of the effect; Villumsen (1985) found heating rates $d\sigma^2/dt$ at a given σ about 6 times lower than the analytical prediction, while Hanninen & Flynn (2002) found rates 3–8 times higher.

Our galaxy formation model predicts the total mass of gas in the disk of each galaxy as a function of time. We assume that the gas is distributed radially in the same way as the stars, with a constant fraction being in the form of giant molecular clouds. For our standard case we will assume that 25% of the gaseous mass of the disk is in clouds (Granato et al. 2000), that they have mass-weighted mean mass of $M_c = 6.6 \times 10^5 M_\odot$ (Lacey 1984) and typical radius $a_c = 16\text{pc}$ (Granato et al. 2000), and that $\beta = 1.5$. For each model galaxy, we integrate the heating due to scattering from molecular clouds over each timestep in the calculations, and add this energy change to that which arises from interactions with satellites.

3 CALIBRATION USING N-BODY SIMULATIONS

As has been noted by several authors, the amount of heating caused by a satellite is difficult to determine analytically since some of the energy may drive global perturbations (e.g. warps) in the disk, and satellites may trigger bar instabilities leading to an enhanced heating rate. Furthermore, our approach to dynamical friction in the disk follows the methods of Chandrasekhar (e.g. Binney & Tremaine 1987, section 7.1), which assume that each particle interacts with the satellite only once. If the satellite orbital period is close to the rotation period of the disk (or to some other resonance of the disk orbits), this assumption fails. Instead, a single particle may interact with the satellite multiple times on consecutive orbits. This problem should therefore ideally be approached in terms of resonant interactions between satellite and disk (Goldreich & Tremaine 1979; Donner & Sundelius 1993; Wahde, Donner & Sundelius 1996; Weinberg & Katz 2002). We retain the Chandrasekhar methods for their simplicity, and show that they provide a reasonable approximation to the dynamical friction due to disks in the regimes of interest.

3.1 N-body Simulations

We begin by testing and calibrating our analytic calculations against numerical simulations of disk heating. In principle, the simulations of VW are ideal for this purpose. However, the central densities and velocity dispersions of the King model satellites given by VW are too low to be consistent with their assumed concentration parameters. Thus, the satellites seem to more weakly bound than the authors intended. It is unclear a priori how this would affect the results and we have therefore decided to repeat their calculations. This has two other advantages:

- We can repeat each simulation without the disk component, allowing us to constrain separately the contributions of the halo and disk to the dynamical friction experienced by the satellite.
- We can perform convergence tests by increasing the number of particles in the simulation in order to ensure that disk heating is being estimated accurately.

We carry out the same set of simulations as VW. Briefly, each simulation consists of a galaxy containing a bulge, disk and dark matter halo, plus a satellite object. Density profiles and the number of particles used for each component are listed in Table 1, while other details of each simulation (type of satellite used, initial satellite orbital parameters and whether or not a disk is included) are listed in Table 2. Initial conditions are created using the techniques of Hernquist (1993). The galaxy and satellite are then evolved separately, as described by VW, using the GADGET code (Springel, Yoshida & White 2001) to allow them to reach equilibrium. We employ GADGET’s new cell-opening criterion for tree walks (`TypeOfOpeningCriteria=1`) with an accuracy of `ErrToIForceAcc=0.001`, together with `TypeOfTimestepCriterion=1` with `ErrToIVelScale=10.0`. GADGET uses adaptive time-stepping. We impose no minimum timestep size, but impose a maximum size of `MaxSizeTimestep=0.01` (in GADGET’s default internal units). All particles in the simulation are given a softening length of 0.110kpc. With these choices, energy is conserved to better than 1% throughout the simulations. The two sets of initial conditions are then superimposed and evolved for 4Gyr.

The simulations are labelled G1S1 to G1S15 as in VW. We also perform a simulation with no satellite, G1S0, to measure the two-body heating rate in the disk. We repeat each simulation without a disk component, labelling these G2S1 to G2S15 (note that in the absence of the disk, only models G2S1, G2S2, G2S7, G2S9 and G2S14 are different). We also repeated all of these calculations with one half and one quarter the number of particles, in order to test how well the results have converged. The convergence tests are described in Appendix D. They indicate that the convergence is good for the evolution of the mass and orbit of the satellite, and adequate for the increase in the vertical energy of the disk. Unless otherwise noted, we show results from the highest resolution simulations.

Each simulation output is analyzed in order to determine the position, velocity and mass of the satellite (computed for those particles which remain bound to the satellite), and the vertical kinetic energy of the disk. We determine which particles are bound to the satellite using the following algorithm:

- Begin by considering all the satellite particles that were bound to the satellite at the previous timestep (or simply all satellite particles for the first timestep).
- Compute the mean position and velocity, and the mass of the satellite from these particles.
- For each particle in this set, determine if it is gravitationally bound to the other particles in the set.
- Retain only those particles which are bound and go

back to step (ii). Repeat until the mass of the satellite has converged.

To determine the vertical kinetic energy of the disk, T_z , at each output time, we first locate the centre of mass of the disk and its mean velocity. (Since the satellite mass is comparable to that of the disk, the disk moves around significantly as the satellite passes by.) We then rotate the system to the frame defined by the principal axes of the disk inertia tensor, and sum the kinetic energies of particles in the direction defined by the shortest axis (which corresponds to the z -axis for an untilted disk). This rotation is necessary because the disk can become tilted through its interaction with the satellite (as also noted by VW). In the original frame (i.e. without rotation), purely circular motions in a tilted disk appear as vertical energy.

One final step is necessary in order to obtain the *increase* in the disk vertical energy due to the interaction with the satellite. Even in the absence of a satellite, the vertical kinetic energy of the disk increases as the simulation proceeds due to numerical relaxation (mainly two-body scattering), from $0.57 \times 10^{14} M_\odot \text{km}^2 \text{s}^{-2}$ at $t = 0$ to $0.64 \times 10^{14} M_\odot \text{km}^2 \text{s}^{-2}$ at $t = 4 \text{Gyr}$, for our standard particle number. This increase of $0.07 \times 10^{14} M_\odot \text{km}^2 \text{s}^{-2}$ due to two-body relaxation is comparable to the heating by the satellite in many of the cases considered. Therefore, to obtain the increase in vertical energy due to the satellite at time t , which we denote as $\Delta T_z(t)$, we subtract off the energy of the unperturbed disk (from model G1S0) at the same time t . Based on runs of model G1S0 with different random number seeds but the same number of particles, the increase in T_z due to numerical relaxation is determined to an accuracy of better than $0.005 \times 10^{14} M_\odot \text{km}^2 \text{s}^{-2}$ in the standard case, so the uncertainty in ΔT_z introduced by the subtraction is small compared to ΔT_z itself.

3.2 Comparison with Analytic Calculations

To test our analytical model of satellite orbital evolution and constrain its parameters, we adapt the analytical model so as to mimic the set-up of each N-body simulation. Thus, we assume density profiles for host and satellite systems identical to those of the N-body simulations. Taylor & Babul (2001) compared their model of satellite galaxy orbital evolution to the orbital radii and satellite masses as a function of time in the simulations of VW, finding generally good agreement. We repeat their analysis here, using our own model of satellite dynamics, extended to include the calculation of disk heating. We will use this comparison to fix the four free parameters of our satellite orbit model, f_{orb} , $f_{\Lambda, \text{h}}$, $f_{\Lambda, \text{d}}$ and ϵ_{h} . As described in Appendix A, f_{orb} controls the timescale on which tidally stripped mass is lost from the satellite, while $f_{\Lambda, \text{h}}$ and $f_{\Lambda, \text{d}}$ are the factors that appear in the Coulomb logarithms, Λ_{h} and Λ_{d} , for the dynamical friction force due to the halo and disk respectively. The parameter ϵ_{h} controls the strength of gravitational shock-heating and is defined in Benson et al. (2002a).

Using our satellite orbit model, each orbit is integrated for 4 Gyr. Figures 2 and 3 show the orbital position and velocity and the remaining bound mass and orbital energy of

the satellite for models G2S2 and G1S3 respectively, with our N-body results shown as open circles. Figure 3 also shows the energy deposited in the disk in model G1S3. This is given by the vertical kinetic energy of the simulated disk minus the vertical kinetic energy of the disk in model G1S0 which contains no satellite. The subtraction removes both the initial energy of the disk, and the energy gained by two-body relaxation during the simulation. We indicate at the top of each figure the label of the satellite model, the initial inclination of the orbit with respect to the galaxy disk (θ_i), the initial circularity (ϵ_{J} ; the angular momentum of the satellite divided by the angular momentum of a circular orbit with the same energy) and the initial apocentric distance of the orbit (r_{a}). Where they are available, we show the results of VW as triangles. Note that in the simulation of VW the satellite loses mass more rapidly, due to the incorrect density profile used. For comparison, we show, as dashed lines, the orbital radius and remaining bound mass derived from the analytical calculations of Taylor & Babul (2001) for the same model.

The results in Figs. 2 and 3 are for the parameter combination $(f_{\text{orb}}, f_{\Lambda, \text{h}}, f_{\Lambda, \text{d}}, \epsilon_{\text{h}}) = (2.5, 1.5, 3.0, 1.0)$. The values of f_{orb} and ϵ_{h} are fixed by matching the mass loss rates found in the simulations with no disk component. The value of $f_{\Lambda, \text{h}}$, which controls the strength of the dynamical friction force due to the halo, is fixed by matching the rate of decay of the orbital radius in models with no disk (so that the orbital decay is caused entirely by the halo plus bulge system). Finally, $f_{\Lambda, \text{d}}$ is fixed by matching the rate of orbital decay in the models which include a disk. In these models, the disk is the dominant source of dynamical friction throughout a substantial fraction of the orbital evolution.

The parameter values that we have selected produce the best agreement with the set of fifteen models that were simulated. Generally, we find quite good agreement with the numerical results, comparable to that achieved by Taylor & Babul (2001)[‡]. Our model uses more general expressions for Λ_{h} and Λ_{d} than that of Taylor & Babul (2001). If we treat those numbers as free parameters (instead of $f_{\Lambda, \text{h}}$ and $f_{\Lambda, \text{d}}$) we are able to achieve even better agreement with the numerical simulations. However, our approach has the advantage that Λ_{d} and Λ_{h} scale in a physically reasonable way when we apply our model to very different satellite/host systems. In any case, orbital positions and velocities are typically matched accurately until the final merging of the satellite (where it becomes difficult to determine these quantities precisely in the N-body simulations). The satellite mass as a function of time is typically matched to within about 30–40%. Table 3 lists several quantities – the final change in the disk energy and the time at which the satellite reaches 50% and 10% of its original mass – from both analytic and N-body calculations for comparison.

It is worth noting that the free parameters of our orbit model are set without reference to the disk heating rate seen

[‡] It should be noted that Taylor & Babul (2001) were attempting to match the simulations of VW, rather than our simulations, so that one should not expect exact agreement of their results with ours.

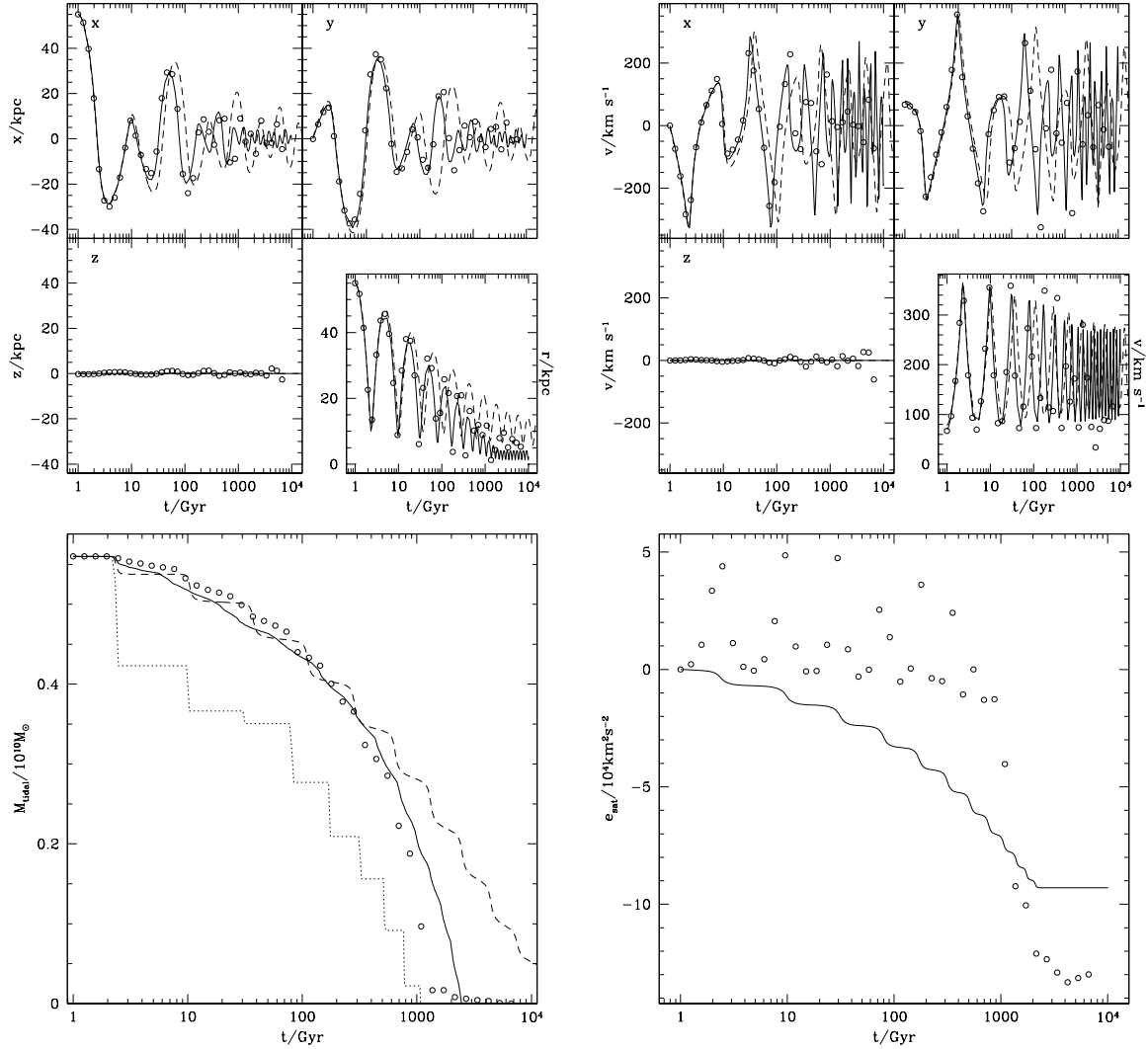
Model G2S2 ($S1$, $\theta_i = 0^\circ$, $\epsilon_J = 0.55$, $r_a = 55\text{kpc}$, no disk)


Figure 2. Evolution of the satellite and its orbit in the diskless model G2S2. We compare the results from our analytical model (solid lines) with the analytical model of Taylor & Babul (2001) (dashed lines) and with our N-body simulation (circles). *Top left-hand panel:* The orbital position and radius of the satellite as a function of time. *Top right-hand panel:* The orbital velocity of the satellite and its components as a function of time. *Lower left-hand panel:* The remaining bound mass of the satellite as a function of time. The dotted line shows the mass of the satellite if mass loss beyond the tidal radius is assumed to occur instantaneously (i.e. $f_{\text{orb}} = 0$). *Lower right-hand panel:* The change in the specific orbital energy of the satellite as a function of time.

in the numerical simulations. Thus, the heating rates we predict are entirely specified by other considerations. The lower right-hand panel in Fig. 3 shows the change in disk vertical kinetic energy from our analytic model calculated as described in §2.2.2 and from the N-body simulation. We find that our analytic model reproduces the final disk energy in the numerical simulations to better than a factor of two in ten out of the fifteen simulations (see Table 3) but, in extreme cases, the difference can be a factor of three or more. Of the five models which do not agree to within a factor of two, one (G1S7) has a prograde satellite orbit in the disk plane ($\theta_i = 0^\circ$), two (G1S4 and G1S11) have polar orbits ($\theta_i = 90^\circ$), and two (G1S8 and G1S10) are on inclined prograde orbits ($\theta_i = 45^\circ$).

For all five of the most discrepant cases, the analytical calculation predicts less heating than the N-body simulation. The largest disagreement occurs for model G1S7 which has a prograde orbit in the disk plane. Here, the analytical determination overestimates the dynamical friction force in the disk as measured in the N-body simulation. The satellite then becomes trapped in an orbit rotating with the disk and there is no further energy transfer to the disk, resulting in an underestimate of the heating in the analytic model by a factor of 8. For the polar orbits (G1S4 and G1S11), mass loss in the analytic model is too rapid and this again reduces the heating rate compared to the N-body calculation. These two models underpredict the N-body heating by a factor of approximately 3. For the inclined orbits (G1S8

Model G1S3 ($S1, \theta_i = 45^\circ, \epsilon_J = 0.55, r_a = 55\text{kpc}$)

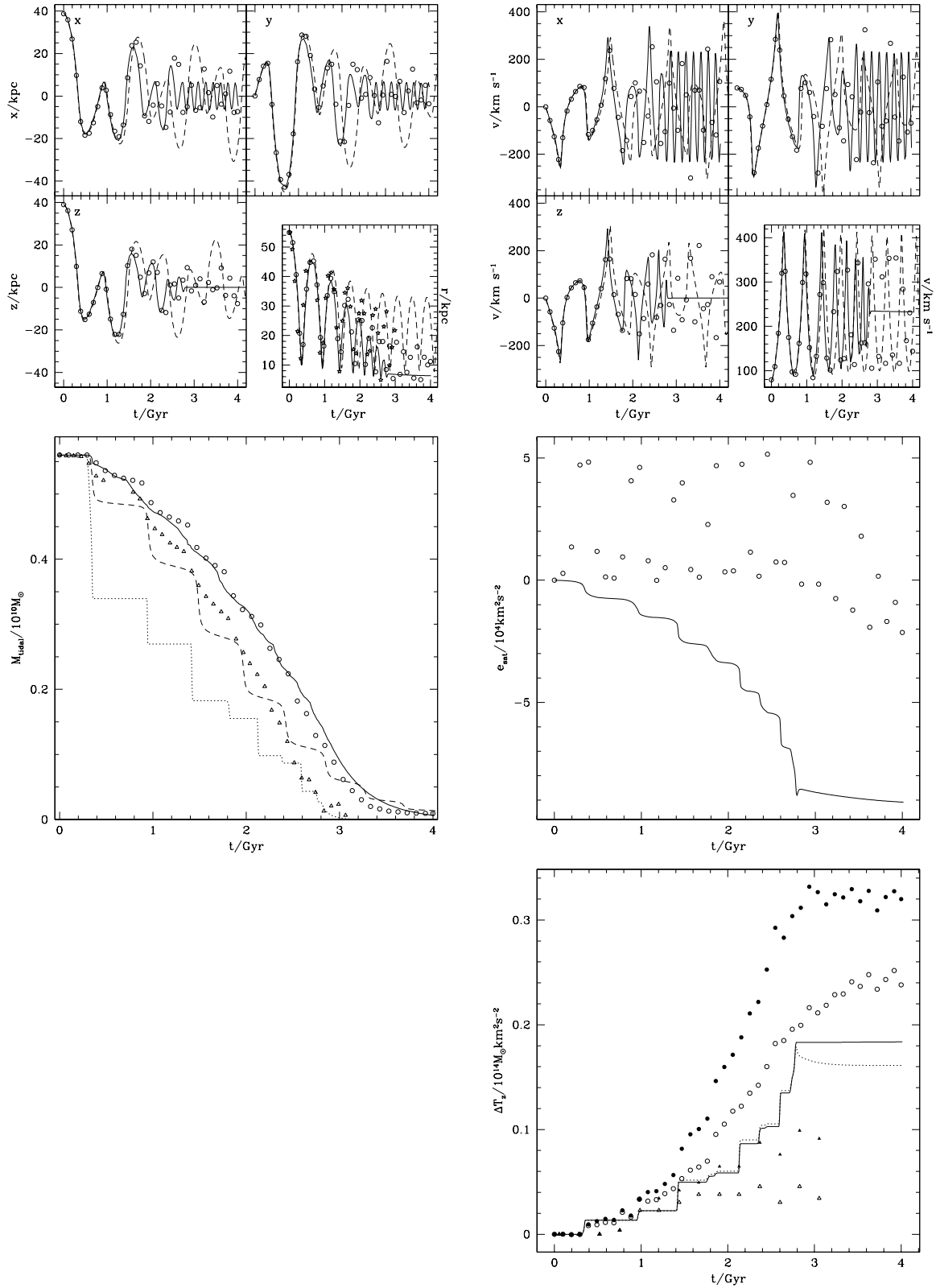


Figure 3.

Figure 3. (*cont.*) Properties of the orbiting satellite and host halo galaxy disk in model G1S3. We compare the results from our analytic calculations (solid lines) and those of Taylor & Babul (2001) (dashed lines), with those from our N-body simulation (circles) and those of Velázquez & White (1999) (triangles). *Top left-hand panel:* The orbital position and radius of the satellite as a function of time. *Top right-hand panel:* The orbital velocity and speed of the satellite as a function of time. *Centre left-hand panel:* The remaining bound mass of the satellite as a function of time. The dotted line shows the mass of the satellite if mass loss beyond the tidal radius is assumed to occur instantaneously. *Centre right-hand panel:* The change in specific orbital energy of the satellite with time. *Lower right-hand panel:* The vertical kinetic energy of the central galaxy disk. Filled symbols show the energy measured in the original coordinate frame of the disk, whereas the open symbols show the energy measured in a frame that coincides with the principal axes of the inertia tensor of the disk at each epoch. The dotted line shows the result obtained if the energies of the disk in each direction (R, ϕ, z) are assumed to reach equipartition.

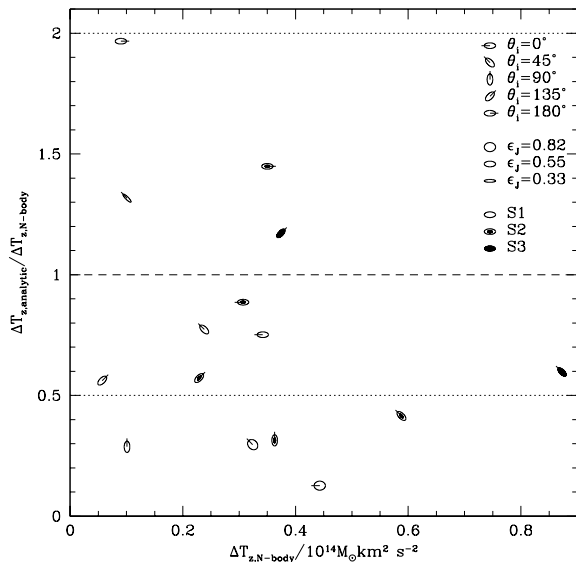


Figure 4. A comparison between the analytic and N-body results for the change in the vertical component of the disk kinetic energy, ΔT_z . The dashed line is the locus of perfect agreement, with the two dotted lines indicating factor of two discrepancies. The symbols, one for each of the fifteen simulations, G1S1 to G1S15, indicate through their orientation, shape and shading the orbital inclination, the orbital circularity and the satellite model respectively.

and G1S10), it is possible that the disk is no longer well described by a single inclination (for example, it may have become warped), leading to an overestimate of the energy in the N-body simulations. (With the number of particles employed in our simulated disks, the inclination of an unwarped disk can be determined to very high precision, so there is very little inaccuracy in the determination of the disk energy).

Figure 4 compares the N-body and analytic results for the change, ΔT_z , in disk kinetic energy. The dashed line is the locus of perfect agreement between the two calculations, and the two dotted lines indicate a factor of two discrepancy. The symbols, one for each of the fifteen simulations, G1S1 to G1S15, indicate through their orientation, shape and shading the orbital inclination, the orbital circularity and the satellite model respectively (as indicated by the key in the figure).

Several of the N-body simulations show evidence of bar

formation in the central regions of the disk. This is particularly evident when the satellite is on a prograde orbit in the disk plane. Bars may be expected to enhance the transfer of energy to the disk, and may be part of the reason why the analytic model (which does not allow for bar formation) substantially underpredicts the amount of heating in some cases (e.g. G1S5 and G1S7, of which the latter shows a particularly strong bar in the N-body simulation).

The efficiency of vertical heating, ϵ_z , is an important component of our calculations. If we did not include this efficiency factor, the predicted heating rates would be up to 4 times higher (depending on the orbit —the effect is largest for near-circular prograde orbits in the disk plane and polar orbits), with a factor of 3 being typical.

The inclusion of the θ dependence in the expression for Λ_d (see Appendix B2.2) tends to reduce the heating rate slightly. The effect is small for most orbits, but it is of greater importance for orbits in the disk plane, helping to improve the agreement with the simulations in those cases. The use of an anisotropic disk velocity dispersion in the dynamical friction force generally has an even smaller effect, typically increasing the disk heating rate by a few percent (although in some cases the rate is decreased by an equally small amount). Prograde orbits in the disk plane are, once again, most strongly affected, with heating rates reduced by 20–40%.

The galaxy in the N-body model contains a bulge of mass 1/3 that of the disk. VW also performed simulations with bulges of mass 1/5 and 2/3 that of the disk to examine the influence of the bulge on the heating rate, finding that a more massive bulge reduced the amount of disk heating. Our analytical model typically reproduces this trend, with approximately the same strength.

To summarize, we are able to reproduce the rates of disk heating seen in numerical simulations for the majority of the cases considered. Where the analytic approach “fails” (we say “fails”, since the N-body techniques have their own inadequacies and do not necessarily represent the correct solution), it underestimates the heating by a factor of 3 on average. In many of the discrepant cases, the incorrect heating rate is a consequence of an incorrect estimate of the disk dynamical friction force or tidal mass loss rate, but in some of the other discrepant cases, the reason is less obvious. It is worth emphasizing that our analytic calculation reproduces several important trends observed in the N-body heating rates. For example:

- heating is greatly suppressed for satellites on polar orbits;
- differences between heating rates for prograde and retrograde orbits (which are not always in the same sense, depending on the satellite type) are reproduced;
- differences due to the concentration or initial mass of the satellite are clearly reproduced.

The trend of increased heating for more circular orbits, seen in the N-body simulations, is not reproduced, however.

While it is clear that the analytic model does not match the N-body heating rates perfectly, in the majority of cases, the differences are compatible with the accuracy of the simulations themselves, as judged by the convergence tests. We conclude that, in general, the analytic model provides a reasonable approximation to the simulation results.

4 RESULTS

4.1 Scale-Height Distribution for Disk Galaxies

Having demonstrated that our model can be used to calculate disk heating rates with reasonable accuracy, we now proceed to apply these calculations to galaxy formation in a cosmological setting. Specifically, we implement this model of disk heating in the GALFORM semi-analytic model of galaxy formation described by Cole et al. (2000) and Benson et al. (2002a), based on a standard Λ CDM cosmology with $\Omega_0 = 0.3$ and $\Lambda_0 = 0.7$ [§]. This model follows the growth of galactic disks in a merging hierarchy of dark matter halos. At each time the model predicts the mass and radial size of the galactic disk forming at the centre of each halo. It also gives the rate at which subhalos are merging into each halo, which we take as input for our calculations of satellite evolution and disk heating. We assume that only direct progenitors of the halo cause heating (i.e. subhalos can heat the disk, but sub-subhalos are not considered). This is to avoid double-counting of mass. We will consider briefly below the effect of allowing all progenitors to heat disks.

Using this model, we generate a representative sample of galaxies living in dark matter halos spanning a wide range of masses. For each galaxy, the model computes the usual properties predicted by this type of modeling (masses, luminosities, etc. —see Cole et al. 2000), and now also the vertical scale-height of the galactic disk. Figures 5 and 6 show the resulting distribution of disk scale-heights, expressed in units of the disk radial scale-length, for galaxies with $M_B - 5 \log h \leq -19.5$ (approximately L_* and brighter galaxies) and $-19.5 < M_B - 5 \log h \leq -17.0$ respectively. We include only spiral galaxies (which we define as any galaxy with a bulge-to-total ratio measured in dust-extinguished B-band light less than 0.4).

We remind the reader that we define the dimensionless scale-height, $h = H_d/R_d$, in terms of the thickness parameter H_d in the sech^2 vertical density law and the ra-

dial exponential scale-length, R_d . The disk thickness can be equivalently defined as $H_d = \Sigma_d/(2\rho_0)$, where Σ_d is the disk surface density and ρ_0 the density at the mid-plane. However, many authors prefer to use the *exponential scale-height* as the measure of disk thickness. Since $\text{sech}^2(z/H_d) \propto \exp(-2z/H_d)$ for $z \gg H_d$, the exponential scale-height that would be measured for our assumed vertical profile is $H_{d,\text{exp}} = H_d/2$.

The left and right-hand panels in Figures 5 and 6 show the scale-height distributions for the global and local heating assumptions, from which we see that the results are not very sensitive to this choice. The figures also show the sensitivity of the results to two other parameters, one numerical and the other physical.

The numerical parameter characterizes the galactocentric radius at which the satellite is assumed to merge with the main galaxy and stop heating the disk. In Cole et al. (2000) and in Paper I, we assumed that two galaxies merge at the time when the separation of their centres, R , equals the sum of their half-mass radii, $R_{\frac{1}{2}\text{sat}} + R_{\frac{1}{2}\text{host}}$. However, once tidal stripping is taken into account, it would seem reasonable to allow the satellite to sink down to $R = 0$ and continue heating the disk while it does so. However, for numerical reasons we cannot integrate the satellite orbits down to $R = 0$. We have therefore calculated the disk heating when the satellite orbit is followed down to $R = f_{\text{heat}}(R_{\frac{1}{2}\text{sat}} + R_{\frac{1}{2}\text{host}})$ for $f_{\text{heat}} = 1, \frac{1}{2}, \frac{1}{4}$ and $\frac{1}{8}$. We find that the distribution of scale-heights has converged for $f_{\text{heat}} = \frac{1}{8}$, and use this as our standard value in what follows. We show in Fig. 5 results for $f_{\text{heat}} = 1$ (dot-dashed lines) and $f_{\text{heat}} = \frac{1}{8}$ (solid lines) in both cases with disk heating by molecular clouds also included. The differences in the scale-height distributions are fairly small (they are somewhat more significant if we do not include disk heating by molecular clouds).

The physical parameter concerns the heating of the disk that results from scattering of stars by giant molecular clouds, computed using eqn. (9). Our standard calculation (solid lines in Figs. 5 and 6) includes heating by clouds with the parameters described in §2.2.5. The figures also show the results when no clouds are present (dotted lines) and when the masses of individual clouds and the fraction of gas in clouds are both doubled (dashed lines). Removing the clouds entirely results in a tail to very low h in the height distribution. These galaxies experienced very little heating by substructures, and so their thickness is almost entirely due to heating by molecular cloud scattering. The peak of the distribution is little changed, but the median scale-height is significantly reduced (see Figure 7). Doubling the cloud mass (dashed lines) results in a shift towards somewhat thicker disks without changing the shape of the distribution.

Global and local heating are found to produce rather similar distributions of scale-heights. Note that we have shown the results for local heating at the disk half-mass radius. Our local heating model, in fact, predicts a trend of increasing scale-height with disk radius; we defer a detailed study of this radial variation to a future paper.

It should be noted that the tails of the distributions extend to $h > 1$, which is clearly unphysical. Our analytical

[§] Benson et al. (2002c) describe small changes in the parameters of this model, relative to those of Benson et al. (2002a), which we retain here.

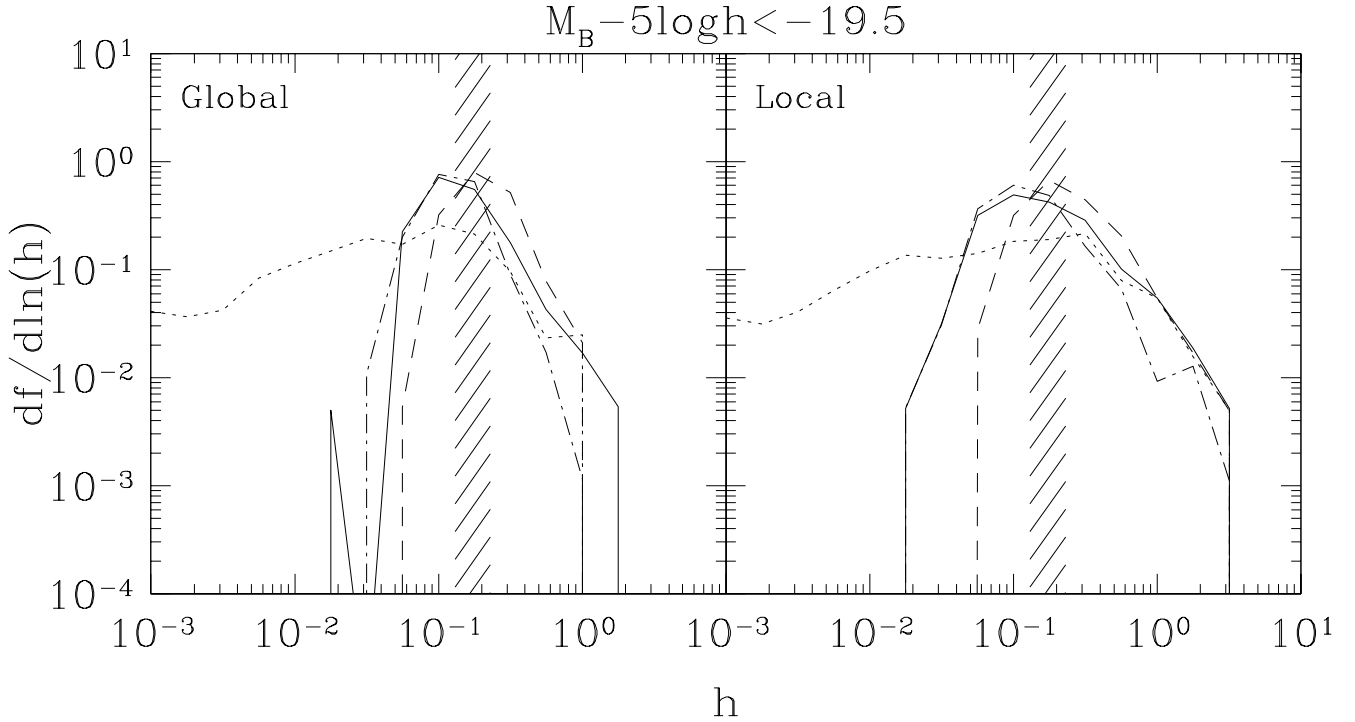


Figure 5. Normalized disk scale-height distributions for spiral galaxies with $M_B - 5 \log h \leq -19.5$. Left and right-hand panels show results for global and local heating respectively. Solid lines show results from our full calculation, including heating from substructure and from scattering by molecular clouds. The dotted line corresponds to ignoring the molecular cloud heating, while the dashed line corresponds to increasing the masses of individual clouds and the total mass in clouds by a factor of two over our standard values. These results correspond to satellite orbits which are integrated until they reach a radius $(R_{\frac{1}{2}\text{sat}} + R_{\frac{1}{2}\text{host}})/8$. For comparison, the dot-dashed line shows the result when the integration is stopped when a radius $(R_{\frac{1}{2}\text{sat}} + R_{\frac{1}{2}\text{host}})$ is reached. The vertical shaded strip shows the observationally allowed range for the scale-height of the Milky Way galaxy, discussed in §4.4.

calculation is based on the thin disk approximation, $h \ll 1$, and so breaks down when $h \sim 1$. We interpret these objects as disks that have been heated so much that they are no longer disks, and must instead resemble a spheroidal or irregular galaxy. For these galaxies, our calculations break down, but we can safely assume that they are no longer recognizable disk galaxies.

4.2 Other Effects on the Scale-Height Distribution

We now discuss tests of various potential systematic effects in our calculations.

Merger Tree Resolution: Our calculations typically resolve dark matter substructures with mass greater than $5 \times 10^9 h^{-1} M_\odot$ in every merger tree. Thus, we ignore the heating due to lower mass halos. Increasing the resolution of to $10^9 h^{-1} M_\odot$ results in no significant increase in the amount of heating experienced by galaxies, indicating that our resolution is sufficient to estimate the total heating rate. (Note that the heating produced by a satellite of mass M should scale approximately as M^2 , making it relatively easy to achieve convergence here provided the number of satellites, $dN/d \ln M$, varies with mass less steeply than

M^{-2} at small mass. In fact, numerical simulations indicate $dN/d \ln M \sim M^{-0.7}$ for subhalos (Springel et al. 2001).)

Effects of Sub-subhalos: In our standard calculation, sub-subhalos (i.e. halos which reside inside a larger halo which subsequently fell into a yet larger halo) do not contribute separately to the heating of disks. (Note that this is different from our treatment of galaxy mergers; the merging times of sub-subhalos are computed from their own properties, not those of the subhalo in which they reside.) An alternative approach would be to treat sub-subhalos (and higher levels of the merging hierarchy) on an equal basis as subhalos. To avoid double-counting of mass in this case, we must remove the mass bound to sub-subhalos when determining the mass of a subhalo. We do this by scaling down the density profile of the subhalo so as to remove this amount of mass before computing heating rates.

If we adopt this approach, we find that the distribution of scale heights is shifted to slightly larger values. Heating by sub-subhalos, however, would only be important if these sub-subhalos survived after their host had been tidally destroyed. While it is unlikely that this would occur to any great extent, numerical simulations could, in principle, answer this question.

Effect of Cosmological Model: Finally, we have repeated

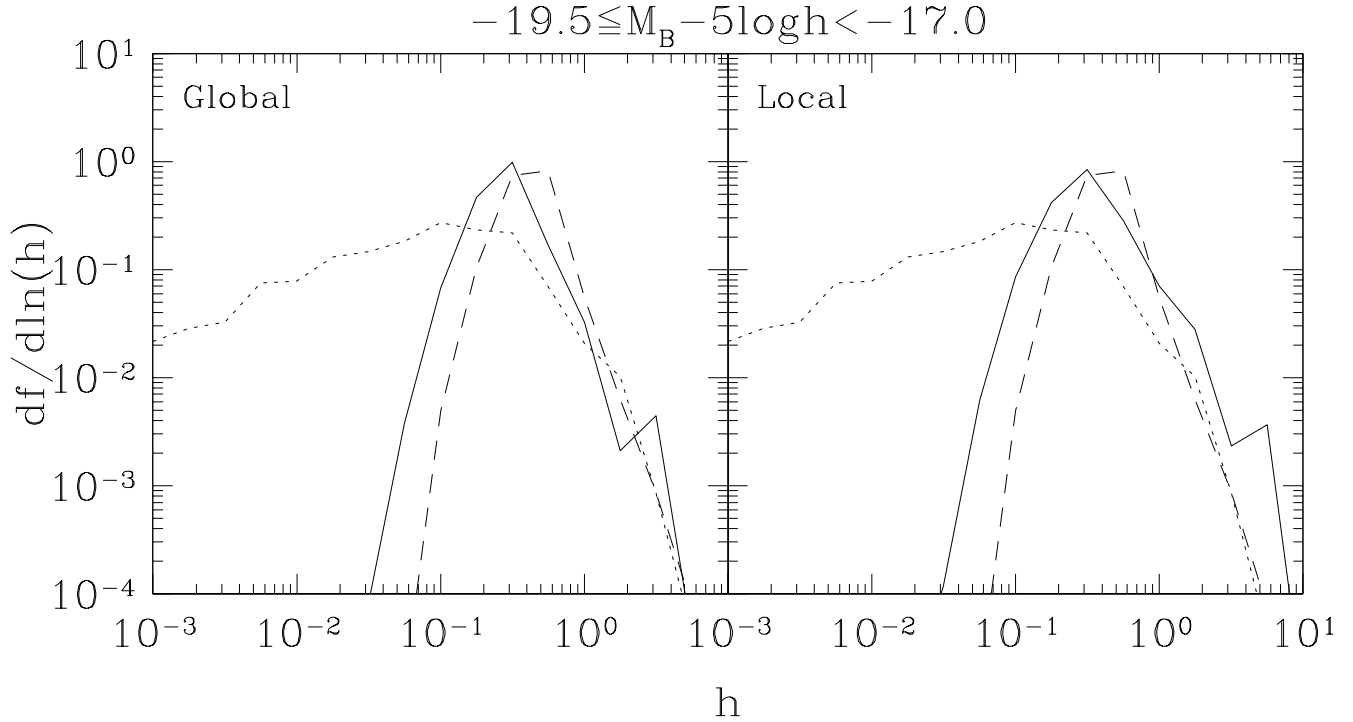


Figure 6. Normalized disk scale-height distributions for spiral galaxies with $-19.5 < M_B - 5 \log h \leq -17.0$. Left and right-hand panels show results for global and local heating respectively. Solid lines show results from our full calculation, including heating from substructure and from scattering by molecular clouds. The dotted line corresponds to ignoring the molecular cloud heating, while the dashed line corresponds to increasing the masses of individual clouds and the total mass in clouds by a factor of two over our standard values.

our calculations in an $\Omega_0 = 1$ cosmology, using the τ CDM parameter set used by Benson et al. (2000a), but including the effects of photoionization suppression[¶]. This model is not as successful at matching the properties of $z = 0$ galaxies as our standard Λ CDM model. In particular, galaxies are somewhat too faint to match the observed luminosity function (by about 0.75 magnitudes in the B-band), forcing us to adopt an unphysical value of the mass-to-light ratio normalization parameter, Υ of 0.7. We find that the median scale-height of L_* disk galaxies is slightly smaller in this cosmology than in our Λ CDM model. At first sight, this seems surprising, since, as noted by TO, there is more infall of substructure at late times in an $\Omega_0 = 1$ cosmology, which would result in a larger rate of heating at the present day. However, our model galaxies in this cosmology are younger than their Λ CDM counterparts (due to the later growth of structure and to the stronger feedback required in this model), and so they have less time in which to be heated. These two effects counteract each other.

The age of our Galactic disk has been estimated using

[¶] Note that Benson et al. (2000a) adopted an artificially high merger rate in order to obtain a good match to the galaxy luminosity functions. With our more detailed model of merging, we no longer have the freedom to adjust the merger rate in this way. We find that, in this cosmology, our revised merger model produces somewhat too few elliptical galaxies.

studies of white dwarfs. For example, Fontaine, Brassard & Bergeron (2001) find an age of 11 Gyr for the Galactic disk. Since they assume a constant star formation rate, this implies a mean stellar age of 5.5 Gyr for the disk stars. Our τ CDM disks typically have a mean stellar age of 4 Gyr, somewhat less than the true value. Consequently, our model underestimates the amount of heating experienced by disks in this cosmology, albeit only by a small factor.

We can understand the similarity of the disk scale-heights in the two cosmologies in more detail by examining the growth histories of the dark matter halos hosting L_* spiral galaxies. In our model, halos of present-day mass $2 \times 10^{12} h^{-1} M_\odot$ have, on average, assembled half of their mass by redshifts of 0.45 and 0.91 respectively in the τ CDM and Λ CDM cosmologies. The mean stellar ages of L_* disk galaxies — 4.0 and 5.5 Gyr for τ CDM and Λ CDM respectively — reflect this difference in halo assembly epoch. We find that the host halos on average accrete close to 25% of their total mass over these galaxy lifetimes in both cosmologies. Therefore, the number of substructures infalling onto a galaxy over its lifetime is roughly the same in both cosmologies, consistent with their similar disk scale-height distributions. It should be kept in mind that the disks in our $\Omega_0 = 1$ model are somewhat unrealistic (e.g. they are too faint for a reasonable Υ and, more importantly, too young). An $\Omega_0 = 1$ model which produced realistic disks might predict larger (or smaller) scale-heights. The important lesson

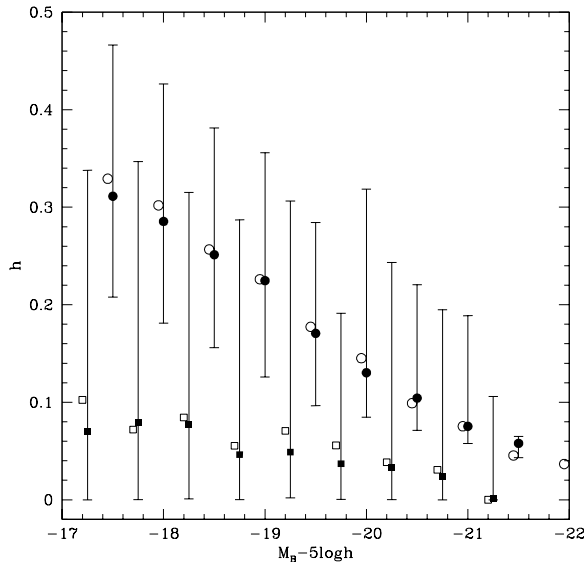


Figure 7. The median fractional scale-heights, $h = H_d/R_d$, of spiral galaxies as a function of absolute magnitude. The squares show the results for heating by substructures only, and the circles for heating by substructures and clouds together. In each case, the filled symbols are for global heating, and the open symbols (offset slightly for clarity) for local heating. The errorbars indicate the 10% and 90% intervals of the distribution of scale-heights. For clarity, the errorbars are suppressed for the local heating case, but are similar to those for global heating.

to derive from these considerations is that disk scale-heights depend on the details of galaxy formation as well as on the cosmological model.

4.3 Scale-Heights as a Function of Luminosity

In Fig. 7, we show the median value of h as a function of absolute magnitude for spiral galaxies in our standard model. The squares show the results for heating by substructure alone, and the circles for heating by substructure and clouds together. The median scale-height at all luminosities is much larger when heating by clouds is included. However, the scatter in scale-height at a given luminosity is extremely large for the case of heating by substructures only, reflecting the strongly stochastic nature of this process. Our calculations predict that brighter galaxies should host thinner disks than fainter galaxies (when measured in terms of the fractional disk thickness, $h = H_d/R_d$). This trend is apparent in calculations with and without molecular clouds, and reflects a similar trend in the fractional vertical energy, $E_z/M_{\text{disk}}V_{\text{disk}}^2$.

4.4 Comparison with the Milky Way galaxy

It has been conventional to compare predictions for disk scale-heights with the observed value for the Milky Way galaxy. As a way of testing models against the real universe, this comparison has significant drawbacks, since (i) the global parameters of the Milky Way (such as the disk

radial scale-length, total luminosity and bulge-to-disk ratio) are, in fact, quite difficult to determine observationally and (ii) the models predict a *distribution* of scale-heights at a given luminosity, and this cannot be constrained well from a single measured point. Therefore, we will make only a brief comparison with the Milky Way here, before comparing with the distribution of scale-heights measured for external galaxies.

The vertical scale-height of the galactic disk in the Solar neighbourhood has been measured from star counts. We use the recent determination by Mendez & Guzman (1998) which, for a $\text{sech}^2(z/H_d)$ vertical profile, gives $H_d = 0.50 \pm 0.08 \text{ kpc}$ (corresponding to an exponential scale-height of $0.25 \pm 0.04 \text{ kpc}$), somewhat smaller than earlier determinations. The measurement of the radial exponential scale-length of the galactic disk has, in the past, been a matter of more disagreement. We use the models of the galactic mass distribution by Dehnen & Binney (1998), which imply $R_d = 3.0 \pm 0.4 \text{ kpc}$. Combining these, we find the fractional scale-height of the Milky Way stellar disk, $h = H_d/R_d = 0.18 \pm 0.05$. This range in h is indicated as a shaded region in Figure 5, from which one can see that the scale-height of the Milky Way is entirely typical of L_* disk galaxies in the model (with 35% of galaxies predicted to have $h > 0.18$). We have repeated the comparison using the same definition of “Milky Way-like” galaxies as in Benson et al. (2002b), namely a circular velocity at the disk half-mass radius between 210–230 km/s and a bulge-to-total ratio by mass between 5–20%. We again find that the observed scale-height of the Milky Way lies well within the distribution of h predicted by the model (with 80% of such galaxies predicted to have $h > 0.18$).

4.5 Comparison with the Observed Scale-Height Distribution for Other Galaxies

The best way to test models of disk heating is by comparing with the observed distribution of scale-heights for external galaxies. This distribution has recently been measured in a complete sample of disk galaxies, for the first time, by Bizyaev & Mitronova (2002). They estimated the vertical and radial scale-lengths of a statistically complete sample of 60 edge-on galaxies using K-band photometry from the 2MASS survey.

We compare the scale-height distribution in Bizyaev & Mitronova (2002) sample with our model predictions in Figure 8. Since the selection criteria for the observational sample are somewhat complex, we weight model galaxies so as to match the distribution of absolute magnitudes in the observational sample (which peaks in the range $-19 < M_B - 5 \log h \leq -18$), and select only those galaxies with bulge-to-total luminosity ratios typical of the morphological types found in the observational sample (which are mostly Sc spirals). We see that the model provides quite a good match to the observed distribution, with both distributions peaking around $h = 0.2$. The only significant discrepancy is that the model predicts too many systems with large $h \gtrsim 0.4$. However, it is not clear that such thick galaxies would be recognized as disk galaxies. The conclusions that can be drawn

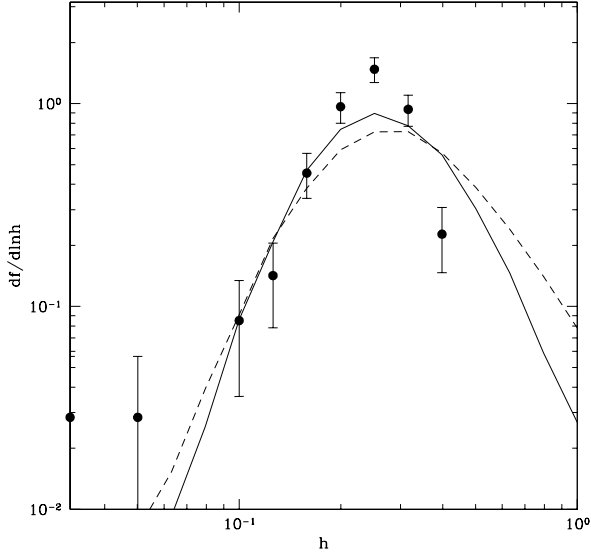


Figure 8. The normalized distribution of scale-heights, h , in the observational sample of Bizyaev & Mitronova (2002) compared to the prediction of our model. Error bars on the observational datapoints indicate Poisson errors. The model predictions are shown by solid and dashed lines for global and local heating respectively. The model galaxies have been weighted to match the distribution of absolute magnitudes and morphological types found in the observational sample.

at present are limited by the relatively small size of the current observational sample. However, this situation should soon improve with the availability of data from large CCD-based sky surveys, which will allow much more thorough tests of the theoretical predictions.

5 DISCUSSION

We have developed a model to calculate the rate of heating of galactic disks by substructures orbiting in their halos. To calibrate the model, we performed N-body simulations of disk heating which we tested for convergence. We find that the analytical model reproduces the heating rates in the N-body simulations to within a factor 3 in most cases. One could perhaps improve the accuracy of the analytical model by treating the satellite–disk interaction in terms of a sum of interactions with resonances in the disk (e.g. Donner & Sundelius 1993; Weinberg & Katz 2002). It is unclear, however, whether such a calculation would ever be worth performing semi-analytically, i.e. whether its computational cost would be any less than that of a full N-body simulation. Nevertheless, it is clear from the calculations presented here that N-body estimates of disk heating rates have their own problems (e.g. very large numbers of particles are required in the disk to determine the heating rate accurately), and so it may yet prove worthwhile to pursue analytical estimates of disk heating.

We find that for galaxy formation in the standard

Λ CDM cosmology, heating by substructure alone produces a distribution of disk scale-heights which is very broad and skewed to low values, with median fractional scale-height, $h = H_d/R_d$, around 0.05 for L_* spiral galaxies. The width of the distribution reflects the stochastic nature of the heating process, which is, in turn, related to the distribution of orbital parameters of the satellites. Including the additional heating generated by stars scattering from gas clouds in the disk increases the median value of h significantly, to around 0.2. The distribution is considerably less broad once the contribution from gas cloud heating is included. Heating by clouds is treated as a deterministic process here, with variations in the amount of heating for a given type of galaxy reflecting the distribution of ages of galactic disks. The fractional scale-height for the Milky Way galaxy, estimated observationally to be around 0.2, is then entirely consistent with our model expectations for a typical L_* spiral galaxy. We find that the predicted distribution of scale-heights for slightly sub- L_* spiral galaxies agrees remarkably well with a recent observational determination by Bizyaev & Mitronova (2002) based on data from the 2MASS survey.

It is intriguing that for the L_* galaxies considered here, satellites and gas clouds give rise to comparable amounts of disk heating. A simple order of magnitude estimate of the scale-heights produced by these two processes illustrates why this is so. Using the expressions given in this paper, we find (for parameter values typical of Milky Way-like galaxies) that the fractional scale-height generated by scattering from giant molecular clouds is

$$h = 7.2 \times 10^{-3} \left[\frac{f}{0.025} \right]^{1/2} \left[\frac{M_c/M_d}{3 \times 10^{-5}} \right]^{1/2} \left[\frac{\ln \Lambda}{3} \right]^{1/2} \\ \times \left[\frac{\nu}{90 \text{ Gyr}^{-1}} \right]^{1/2} \left[\frac{\alpha_S(\beta)}{0.7} \right]^{3/2} \left[\frac{K_S(\beta)}{0.15} \right]^{1/2} \left[\frac{t}{\text{Gyr}} \right]^{1/2} \quad (11)$$

while that generated by dark matter substructures is

$$h = 0.16 \left[\frac{f_{\text{mass}}}{0.1} \right] \left[\frac{f_{\text{max}}}{0.01} \right] \left[\frac{\epsilon_z}{0.3} \right] \left[\frac{M_{\text{halo}}}{10^{12} M_\odot} \right]^2 \left[\frac{\ln \Lambda}{3} \right] \\ \times \left[\frac{V_s}{200 \text{ km/s}} \right]^{-1} \left[\frac{R_d}{3.5 \text{ kpc}} \right]^{-1} \left[\frac{r_{\text{orb}}}{200 \text{ kpc}} \right]^{-1} \\ \times \left[\frac{M_d}{5 \times 10^{10} M_\odot} \right]^{-1} \left[\frac{t}{\text{Gyr}} \right] \quad (12)$$

In the first equation, f is the fraction of the total disk mass in the form of giant molecular clouds. In the second equation, V_s is the typical orbital velocity of satellites, r_{orb} their typical orbital radius, f_{mass} is the fraction of the total halo mass in the form of substructures, f_{max} is the mass of the largest substructure in units of the total halo mass and we have assumed a distribution of substructure masses $dN/dM \propto M^{-1.7}$. In both cases t is the time for which heating has occurred. To derive the second expression, we have assumed that substructures heat the disk only over a fraction of their orbit approximately equal to H_d/r_{orb} . Taking $t \approx 10$ Gyr, these estimates imply $h \sim 0.1 - 1$ for both heating mechanisms, confirming the coincidence that the two contribute approximately equally to the scale-height of Milky Way-like disks (given the crude approximations made

above and the fact that we have ignored the stochastic nature of heating by satellites). However, these two expressions have different dependencies upon the properties of the galaxies in question. Thus, we should not expect the two to make equal contributions to the scale-height of galaxies dissimilar to the Milky Way. This may be seen in Fig. 7, where it is clear that the heating by substructures is relatively less important for lower luminosity galaxies. In conclusion, the fact that the two heating mechanisms make similar contributions to the scale-heights of Milky Way-like galaxies appears to be coincidental.

It is interesting to compare our conclusions with those of TO, who found that the Milky Way disk could have accreted only up to 5% of its mass within the Solar circle within the past 5 Gyr without becoming too thick. Our calculations show that the Milky Way halo in fact accreted around 25% of *its* mass (i.e. the total dark mass of the halo) during this time. This is approximately 100 times more than the TO limit. Disks in our model are able to remain fairly thin despite this substantial accretion for two reasons. Firstly, many of the accreted subhalos have orbits which do not take them close to the central galaxy disk, and so they contribute almost nothing to the heating of the disk. Figure 9 shows the amount of energy transferred to the disk of a Milky Way-like galaxy by individual dark matter satellites as a function of their mass. At a fixed mass, the distribution of heating energies has a bimodal distribution. Virtually all of the heating energy is supplied by the satellites in the upper branch which are those whose orbits take them close to the central galaxy disk. These satellites are “trapped” by dynamical friction and damage the disk during an extended period; distant satellites, on the other hand, have a negligible effect. The satellites that cause most of the heating amount to only 6% by mass. Thus, of the $5 \times 10^{11} M_{\odot}$ infalling, only around $3 \times 10^{10} M_{\odot}$ contribute to heating the disk. This is still 6 times larger than the TO limit ($0.5 \times 10^{10} M_{\odot}$).

The second difference with TO is that we find that tidal mass loss in subhalos substantially reduces the amount of heating experienced by the disk. This is in disagreement with TO, who found that tidal mass loss reduced disk scale-heights by at most a factor of two. If we do not allow satellites to lose mass, the peak of the scale-height distribution is shifted to a value of h which is approximately ten times larger than our standard result. This, of course, reflects the different density profiles that we assign to both the host and satellite halos (and which are significantly more extended than the objects considered by TO), and the associated increase in the dynamical friction timescale in our model. In conclusion, our results are in partial agreement with those of TO—halos in our model accrete much more mass in the past 5 Gyr than the TO limit, but little of this mass ever contributes to heating the disk.

There is clearly a need for further study of the heating of galactic disks. In particular, the importance of heating by satellite-triggered bars and the extent to which heating is local or global are important, yet poorly understood aspects of the problem. We believe that analytical modeling of the type developed in this paper provides a powerful means by which to estimate the degree of heating by substructures and could

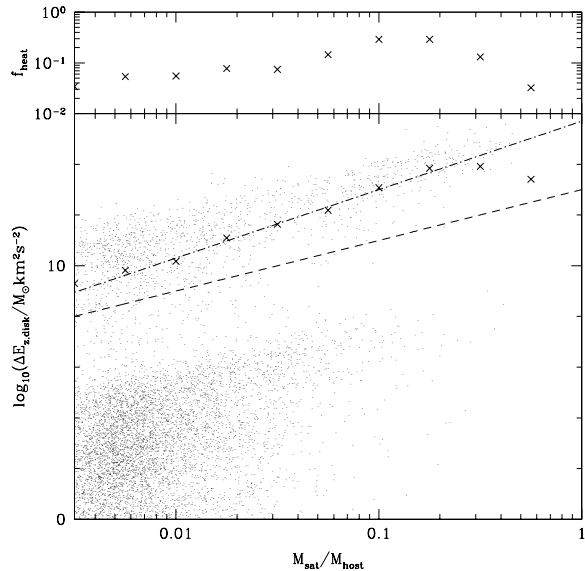


Figure 9. The energy contributed to disk heating by satellites as a function of their mass is shown in the lower panel. Points show the results for a large sample of satellites, for which we plot the heating energy supplied ($\Delta E_{z,\text{disk}}$) against the mass of the satellite (expressed in units of the mass of the host system halo). At fixed mass, the distribution shows a bimodal form, the dashed line indicates the approximate division between the two peaks of the distribution. Crosses indicate the mean heating energy per satellite at each mass, and the dot-dashed line shows an approximate fit to these points. In the upper panel, we show the fraction of points at each mass which lie above the dashed line in the lower panel.

easily incorporate any improvements in our understanding of the physics of the process. Its particular strengths are the ability to resolve fully all substructures contributing to the heating and to compute many realizations of the heating process rapidly, thus allowing the full distribution of scale-heights to be determined. These features have allowed us to present predicted distributions of galaxy scale-heights which will be tested by forthcoming observational data.

In conclusion, the observed thickness of the Milky Way’s stellar disk seems to be entirely consistent with the amount of substructure in galactic halos expected in a cold dark matter universe. Stars scattering from giant molecular clouds and substructures passing through or near the disk produce similar amounts of heating. Distinguishing these two contributions observationally might be possible by means of the stellar age-velocity dispersion relation in the Milky Way disk. An important extension of this work will therefore be to examine model predictions for heating as a function of time within individual galaxies. The lowest values of h for disk galaxies are set by the heating due to star-cloud interactions, while the highest values are set by the heating due to substructures. Thus, precise measurements of the disk scale-height distribution can potentially constrain these two processes.

ACKNOWLEDGMENTS

We thank Peter Goldreich, Chung-Pei Ma, Milos Milosavljevic and Simon White for enlightening discussions, James Taylor for providing results from his satellite orbit calculations in electronic form, Volker Springel for making his GADGET N-body code publically available and the anonymous referee for many valuable suggestions. AJB acknowledges the hospitality of the University of Durham and the Kavli Institute for Theoretical Physics where much of this work was completed. AJB and CMB acknowledge receipt of Royal Society University Research Fellowships. CGL was supported at Durham by the PPARC rolling grant in Cosmology and Extragalactic Astronomy. This research was supported in part by the National Science Foundation under Grant No. PHY99-07949.

REFERENCES

- Benson A. J., Cole S., Frenk C. S., Baugh C. M., Lacey C. G., 2000a, *MNRAS*, 311, 793
 Benson A. J., Lacey C. G., Baugh C. M., Cole S., Frenk C. S., 2002a, *MNRAS*, 333, 156
 Benson A. J., Frenk C. S., Lacey C. G., Baugh C. M., Cole S., 2002b, *MNRAS*, 333, 177
 Benson A. J., Lacey C. G., Baugh C. M., Cole S., Frenk C. S., 2002c, *MNRAS*, 343, 679
 Binney J., 1977, *MNRAS*, 181, 735
 Binney J., Tremaine S., 1987, “Galactic Dynamics”, Princeton University Press, Princeton
 Bizyaev D., Mitronova S., 2002, *A&A*, 389, 795
 Bontekoe T. R., van Albada T. S., 1987, *MNRAS*, 224, 349
 Bullock J. S., Kravtsov A. V., Weinberg D. H., 2000, *ApJ*, 539, 517
 Carlberg R. G., Sellwood J. A., 1985, *ApJ*, 292, 79
 Chiba M., 2002, *ApJ*, 565, 17
 Cole S., Lacey C. G., Baugh C. M., Frenk C. S., 2000, *MNRAS*, 319, 168
 Colpi M., Mayer L., Governato F., 1999, *ApJ*, 525, 720
 Cora S. A., Muzzio J. C., Vergne M. M., 1997, *MNRAS*, 289, 253
 Dalal N., Kochanek C. S., 2002a, *ApJ*, 572, 25
 Dalal N., Kochanek C. S., 2002b, submitted to *ApJ* (astro-ph/0202290)
 de Grijs R., Peletier R. F., 1997, *A&A*, 320, L21
 Dehnen W. & Binney J., 1998, *MNRAS*, 294, 429.
 Donner K. J., Sundelius B., 1993, *MNRAS*, 265, 88
 Font A. S., Navarro J. F., Stadel J., Quinn T., 2001, *ApJ*, 563, L1
 Fontaine G., Brassard P., Bergeron P., 2001, *PASP*, 113, 409
 Ghigna S., Moore B., Governato F., Lake G., Quinn T., Stadel J., 1998, *MNRAS*, 300, 146
 Goldreich P., Tremaine S., 1979, *ApJ*, 233, 857
 Granato G. L., Lacey C. G., Silva L., Bressan A., Baugh C. M., Cole S., Frenk C. S., 2000, *ApJ*, 542, 710
 Hanninen J. & Flynn C., 2002, *MNRAS*, 337, 731
 Hernquist L., 1993, *ApJS*, 86, 389
 Huang S., Carlberg R. G., 1997, *ApJ*, 480, 503
 King I. R., 1966, *AJ*, 71, 64
 Klypin A. A., Kravtsov A. V., Valenzuela O., Prada F., 1999, *ApJ*, 522, 82
 Lacey C. G., 1984, *MNRAS*, 208, 687
 Lewis J. R., Freeman K. C., 1989, *AJ*, 97, 139
 Mao S., Schneider P., 1998, *MNRAS*, 295, 587
 Mendez R. A. & Guzman R., 1998, *A&A*, 333, 106
 Metcalf R. B., Madau P., 2001, *ApJ*, 563, 9
 Moore B., 2001, in J. C. Wheeler and H. Martel eds. “20th Texas Symposium on Relativistic Astrophysics”, AIP Conference Proceedings, Vol 586, p. 73
 Moore B., Ghigna S., Governato F., Lake G., Quinn T., Stadel J., Tozzi P., 1999, *ApJ*, 524, L19
 Navarro J., Frenk C.S. & White S.D.M., 1994, *MNRAS*, 267, L1
 Siegel M. H., Majewski S. R., Reid I. N., Thompson I. B., 2002, *ApJ*, 578, 151
 Somerville R. S., 2002, *ApJ*, 572, 597
 Spitzer L., Schwarzschild M., 1953, *ApJ*, 118, 106
 Springel V., Yoshida N., White S. D. M., 2001, *NewA*, 6, 79
 Springel V., White S. D. M., Tormen G., Kauffmann G., 2001, *MNRAS*, 328, 726
 Taffoni G., Mayer L., Colpi M., Governato F., 2003, *MNRAS*, 341, 434
 Taylor J. E., Babul A., 2001, *ApJ*, 559, 716
 Taylor J. E., Babul A., 2003, submitted to *MNRAS* (astro-ph/0301612)
 Tóth G., Ostriker J. P., 1992, *ApJ*, 389, 5
 van den Bosch F. C., Lewis G. F., Lake G., Stadel J., 1999, *ApJ*, 515, 50
 Velázquez H., White S. D. M., 1999, *MNRAS*, 304, 254
 Villumsen J. V., 1985, *ApJ*, 290, 75
 Wahde M., Donner K. J., Sundelius B., 1996, *MNRAS*, 281, 1165
 Weinberg M. D., 1986, *ApJ*, 300, 93
 Weinberg M. D., Katz N., 2002, *ApJ*, 580, 627

APPENDIX A: IMPROVEMENTS IN THE SATELLITE EVOLUTION MODEL

We detail here the changes in the model of satellite evolution presented in Paper I.

i) As before, that mass of a satellite which has become unbound due to tidal forces is lost gradually over a time comparable to the orbital period. The fraction of the unbound mass lost in a small timestep of duration δt was chosen to be proportional to $\delta t/t_{\text{orb}}$, where t_{orb} is an estimate of the orbital timescale. In Paper I, we chose $t_{\text{orb}} = 2\pi/\omega$, where ω is the instantaneous angular velocity of the satellite. In the present work, we instead take $t_{\text{orb}} = f_{\text{orb}}2\pi/\sqrt{\omega_{\text{peri}}\omega_{\text{apo}}}$, where ω_{peri} and ω_{apo} are the angular velocity of the satellite at its most recent pericentric and apocentric passages, and f_{orb} is an adjustable parameter which we expect to be of order unity. (Prior to the first pericentric passage we revert to our previous definition of mass loss timescale — this makes little difference to our results as typically very little mass loss occurs prior to this time.) The advantage of this choice is that it produces smoother mass loss histories (as is shown in §4). Furthermore, when considering cosmological distributions of satellites, we occasionally find orbits which are near-radial. The above definition then prevents the mass loss rate from becoming arbitrarily small.

ii) In Chandrasekhar’s formula for the dynamical friction force, Taylor & Babul (2001) adopted fixed Coulomb logarithms of $\ln \Lambda = 2.4$ for the dynamical friction force due to the combined halo/bulge system and $\ln \Lambda = 0.5$ for the force due to the disk. They found that these values resulted in the best match to the results of the numerical simulations of Velázquez & White (1999; hereafter VW), and we

adopted the same values in Paper I. Since we will be interested here in a wide range of satellite and host halo masses, we adopt more general definitions. For the halo and bulge systems we take $\Lambda_h = f_{\Lambda,h} r (v_{\text{sat}}^2 + \sigma_{1D}^2) / GM_{\text{sat}}$, where r is the orbital radius of the satellite, M_{sat} its mass, v_{sat} the orbital velocity of the satellite, σ_{1D} the one dimensional velocity dispersion of the halo at radius r , and $f_{\Lambda,h}$ is a parameter. Since $\Lambda_h \leq 1$ is possible with this definition, we replace the usual $\ln \Lambda_h$ term in the expression for the dynamical friction force (eqn. 20 of Paper I) with $\frac{1}{2} \ln(1 + \Lambda_h^2)$, the correct form for small Λ_h (Binney & Tremaine 1987). We also account for the finite size of the satellite as described in Appendix B2. For the disk we must account for the differing scale-lengths in the radial and vertical directions. A suitable expression for the Coulomb logarithm is derived in Appendix B2.2, and depends on the disk scale-length and velocity dispersions, the velocity of the satellite relative to the disk, the angle this velocity makes with the disk plane, and on a parameter, $f_{\Lambda,d}$ which plays a similar role to $f_{\Lambda,h}$. These forms are used throughout our calculations.

iii) The disk is now treated as having an anisotropic velocity dispersion ($\sigma_R, \sigma_\phi, \sigma_z$) in the radial, azimuthal and vertical directions, and this anisotropy is included in the calculation of the dynamical friction force due to the disk (see Appendix B2.1). We adopt essentially the same model for the disk velocity dispersion components as VW. For the radial velocity dispersions, we set $\sigma_R^2 \propto \exp(-R/R_d)$ (Lewis & Freeman 1989)^{||}, where R_d is the disk radial scale-length, and fix the normalization by assuming the disk to have a Toomre Q -parameter of 1.5 at its half-mass radius, which results in $Q \approx 1.5$ at the Solar radius in a Milky Way-like galaxy disk (VW). The azimuthal velocity dispersion is then determined using the epicyclic approximation, $\sigma_\phi^2 = \sigma_R^2 \kappa^2 / 4\Omega^2$ (where κ is the epicyclic frequency and Ω the orbital frequency of the disk). The vertical velocity dispersion at each radius is calculated from the vertical scale-height H_d , assumed constant with radius, using the expressions in §2.2.2 (the vertical scale-height in turn is related to the disk vertical energy). In the analytical disk-heating calculation, the radial and azimuthal velocity dispersions are kept fixed in time, but the vertical velocity dispersion evolves with the disk vertical energy.

iv) When computing the dynamical friction force due to the disk, we smooth the disk density to account for the finite size of the satellite halo as did Taylor & Babul (2001). We smooth on a scale equal to the current radius of the satellite after tidal limitation and gravitational shock-heating.

v) As the disk scale-height will increase as a function of time due to disk heating, we allow for a variable disk scale-height in our satellite orbit calculations. This affects both the dynamical friction force due to the disk and also the gravitational forces exerted by the disk.

vi) Heating by gravitational shocks causes shells of material within a satellite to expand before they become completely unbound. Previously, this effect was included in the

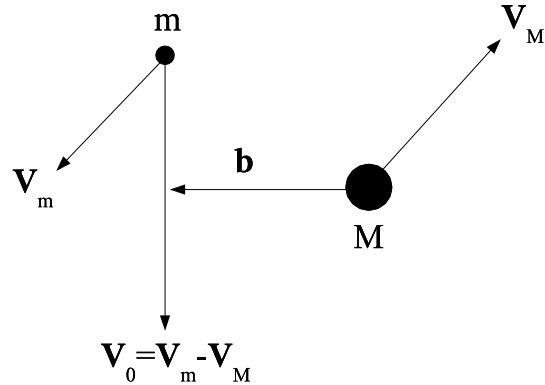


Figure B1. The geometry of a scattering event contributing to the dynamical friction force on mass M (the satellite) due to a particle of mass m (a background particle). Here, V_M and v_m are the velocities of M and m respectively, while V_0 is the relative velocity of the two and b is the impact parameter for this scattering event.

calculation of the tidal mass loss, but not in the calculation of the final internal structure. We now calculate the evolution of the internal density and circular velocity profile assuming that the radii of shells of dark matter scale in inverse proportion to their energy. We have repeated the comparison we performed in Paper I of the distribution of peak internal circular velocities of satellite halos predicted by the semi-analytical model with the results of cosmological N-body simulations. We find that the same choice of initial satellite orbital parameters as in Paper I still gives the best match to the N-body simulations.

APPENDIX B: DYNAMICAL FRICTION FORMULAE

In this appendix we derive several formulae related to dynamical friction which are employed in this work. For completeness, in §B1 and §B2 we derive several well-known relations relevant to dynamical friction. A more complete discussion of these results can be found in Binney & Tremaine (1987) for example. We consider a mass M moving through an infinite and homogeneous sea of particles of mass $m (\ll M)$, number density n and density $\rho = mn$.

B1 Single Scattering Events

For a single scattering event we take the results of Binney & Tremaine (1987; page 422). The scattering geometry is illustrated in Fig. B1. The changes in M 's velocity parallel

^{||} Note that VW contains an error in this equation, although the text of that paper is correct.

and perpendicular to the initial relative velocity vector of the m and M , \mathbf{V}_0 , are:

$$\Delta \mathbf{V}_{\parallel} = \frac{2m}{M} \left[1 + \frac{b^2 V_0^4}{G^2 M^2} \right]^{-1} \mathbf{V}_0, \quad (\text{B1})$$

and

$$\Delta \mathbf{V}_{\perp} = \frac{2m V_0^3}{G M^2} \left[1 + \frac{b^2 V_0^4}{G^2 M^2} \right]^{-1} \mathbf{b}, \quad (\text{B2})$$

where b is the impact parameter and we have assumed the background particles to be much less massive than the object for which the force is being calculated.

B2 Rate of Change of Velocity

We now envisage a sea of particles m with a distribution of velocities given by $f(\mathbf{V}_m)$. The contribution to the rate of change of velocity in the parallel direction from particles with velocity \mathbf{V}_m is simply

$$\frac{d\mathbf{V}_{\parallel}}{dt} = f(\mathbf{V}_m) \int_0^{b_{\max}} 2\pi b n \mathbf{V}_0 \Delta V_{\parallel} db. \quad (\text{B3})$$

This gives,

$$\frac{dV_{\parallel}}{dt} = 2\pi \ln(1 + \Lambda^2) \rho G^2 M f(\mathbf{V}_m) \frac{\mathbf{V}_0}{V_0^3}, \quad (\text{B4})$$

where $\Lambda = b_{\max} V_0^2 / GM$. If M has a finite extent (corresponding to replacing the lower integration limit of 0 with b_{\min}), the above equation still holds with an effective Λ given by

$$\Lambda_{\text{eff}} = \left(\frac{1 + \Lambda^2}{1 + [b_{\min}/b_{\max}]^2 \Lambda^2} - 1 \right)^{1/2}. \quad (\text{B5})$$

Throughout this work, we take b_{\min} equal to half the current tidal radius of the satellite.

Clearly, the net change in the velocity of M perpendicular to \mathbf{V}_0 is zero by symmetry. Thus, the net rate of change of velocity of M is

$$\frac{d\mathbf{V}_M}{dt} = 2\pi \ln(1 + \Lambda^2) \rho G^2 M \int f(\mathbf{V}_m) \frac{(\mathbf{V}_m - \mathbf{V}_M)}{(\mathbf{V}_m - \mathbf{V}_M)^3} d^3 \mathbf{V}_m. \quad (\text{B6})$$

The integral in the above equation has an identical form to integrals used to find the gravitational force at position x_0 due to a density distribution, if we identify $f(\mathbf{V}_m) \equiv G\rho(\mathbf{x})$, $\mathbf{V}_m \equiv \mathbf{x}$ and $\mathbf{V}_M \equiv \mathbf{x}_0$.

Thus, the power extracted from the body through dynamical friction is given by,

$$\begin{aligned} P_{\text{scat}} &= M \mathbf{V}_M \cdot \frac{d\mathbf{V}_M}{dt} \\ &= 2\pi \ln(1 + \Lambda^2) \rho G^2 M^2 \\ &\quad \mathbf{V}_M \cdot \int f(\mathbf{V}_m) \frac{(\mathbf{V}_m - \mathbf{V}_M)}{(\mathbf{V}_m - \mathbf{V}_M)^3} d^3 \mathbf{V}_m. \end{aligned} \quad (\text{B7})$$

B2.1 Application to an Arbitrary Velocity Ellipsoid

Binney (1977) derives an expression for the dynamical friction force due to a system of particles with uniform density

and Gaussian velocity distribution with dispersion σ_{\perp} in one direction and σ_{\parallel} in the other two directions. Binney's equation (A4) is trivially generalized to the case where the velocity dispersions differ in all three directions. Combining this with his equation (A3) we find the following expression for the dynamical friction force:

$$\begin{aligned} \mathbf{F}_{\text{df}} &= \sqrt{2\pi} \ln(1 + \Lambda^2) \rho G^2 M^2 \frac{\sqrt{(1 - e_{\phi}^2)(1 - e_z^2)}}{\sigma_R \sigma_{\phi} \sigma_z} \\ &\quad \times (B_R v_R \hat{\mathbf{e}}_R + B_{\phi} v_{\phi} \hat{\mathbf{e}}_{\phi} + B_z v_z \hat{\mathbf{e}}_z) \end{aligned} \quad (\text{B8})$$

where ρ is the background density, M the mass of the orbiting object, (v_R, v_{ϕ}, v_z) is the relative velocity vector of object and background particles (in cylindrical polar coordinates since we will apply this expression to a galaxy disk), $\hat{\mathbf{e}}_R, \hat{\mathbf{e}}_{\phi}, \hat{\mathbf{e}}_z$ are the basis vectors of the cylindrical polar coordinate system. The coefficients B are given by,

$$\begin{aligned} B_R &= \int_0^{\infty} \frac{dq}{[(1+q)^3(1-e_{\phi}^2+q)(1-e_z^2+q)]^{1/2}} \\ &\quad \times \exp\left(-\frac{1}{2} \left[\frac{v_R^2/\sigma_R^2}{(1+q)} + \frac{v_{\phi}^2/\sigma_R^2}{(1-e_{\phi}^2+q)} \right. \right. \\ &\quad \left. \left. + \frac{v_z^2/\sigma_R^2}{(1-e_z^2+q)} \right] \right), \end{aligned} \quad (\text{B9})$$

$$\begin{aligned} B_{\phi} &= \int_0^{\infty} \frac{dq}{[(1+q)(1-e_{\phi}^2+q)^3(1-e_z^2+q)]^{1/2}} \\ &\quad \times \exp\left(-\frac{1}{2} \left[\frac{v_R^2/\sigma_R^2}{(1+q)} + \frac{v_{\phi}^2/\sigma_R^2}{(1-e_{\phi}^2+q)} \right. \right. \\ &\quad \left. \left. + \frac{v_z^2/\sigma_R^2}{(1-e_z^2+q)} \right] \right), \end{aligned} \quad (\text{B10})$$

$$\begin{aligned} B_z &= \int_0^{\infty} \frac{dq}{[(1+q)(1-e_{\phi}^2+q)(1-e_z^2+q)^3]^{1/2}} \\ &\quad \times \exp\left(-\frac{1}{2} \left[\frac{v_R^2/\sigma_R^2}{(1+q)} + \frac{v_{\phi}^2/\sigma_R^2}{(1-e_{\phi}^2+q)} \right. \right. \\ &\quad \left. \left. + \frac{v_z^2/\sigma_R^2}{(1-e_z^2+q)} \right] \right), \end{aligned} \quad (\text{B11})$$

where $1 - e_{\phi}^2 = \sigma_{\phi}^2/\sigma_R^2$ and $1 - e_z^2 = \sigma_z^2/\sigma_R^2$.

B2.2 Effective Coulomb Logarithm for the Disk

In calculating the dynamical friction force due to the disk we require the Coulomb logarithm, $\frac{1}{2} \ln(1 + \Lambda^2)$, where Λ is normally defined as $\Lambda = b_{\max} V_0^2 / GM$, where V_0 is the typical relative velocity of the satellite and stars in the disk. We adopt $V_0^2 = V_{\text{rel}}^2 + (\sigma_R^2 + \sigma_{\phi}^2 + \sigma_z^2)/3$, where V_{rel} is the relative velocity of the satellite and the bulk disk motion, and σ_R, σ_{ϕ} and σ_z are the three components of the disk velocity dispersion.

When computing the dynamical friction force we sum the contributions from all particles with impact parameter b by integrating around an annulus of radius b normal to the relative velocity vector of the particles and the satellite. We define ψ as the angle of a point on this annulus measured from a vector, \mathbf{p} , which lies in the plane of the annulus and which is parallel to the disk plane (see Fig. B2).

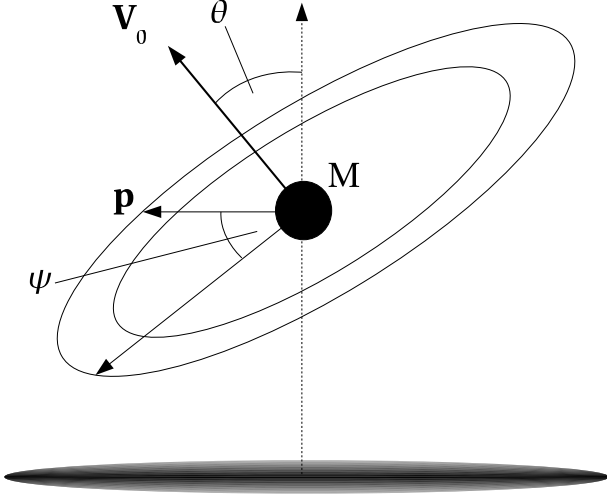


Figure B2. The geometry used in calculating the Coulomb logarithm for the disk. Scatterings through an annulus normal to \mathbf{V}_0 (the relative velocity of satellite and disk stars) are considered. \mathbf{p} is a vector lying in this annulus and parallel to the galaxy disk. Angles in the annulus, ψ , are measured from \mathbf{p} . Finally, θ is the angle between \mathbf{V}_0 and the normal to the disk.

For the disk, the value of b_{\max} , the upper limit of integration in eqn. (B3), will vary as a function of ψ . In the direction corresponding to $\psi = 0$ (and $\psi = \pi$) the disk density distribution has a characteristic length-scale of R_d (the exponential scale-length). This will therefore correspond (approximately) to the largest impact parameter scatterings occurring in that direction. In perpendicular directions ($\psi = \pi/2$ and $\psi = 3\pi/2$) a more appropriate characteristic length is $r_{\text{eff}} = R_d(\cos^2 \theta + h^2 \sin^2 \theta)^{1/2}$, where θ is the angle between the satellite-disk relative velocity vector and the z -axis, and h the ratio of disk scale-height to scale-length. Thus, the effective Λ in direction ψ is

$$\Lambda = \frac{f_{\Lambda,d} R_d h' V_0^2}{GM}, \quad (\text{B12})$$

where $h' = (\cos^2 \psi + [\cos^2 \theta + h^2 \sin^2 \theta] \sin^2 \psi)^{1/2}$. If we account for the finite size of the satellite then:

$$(1 + \Lambda^2)_{\text{eff}} = \frac{1 + \Lambda^2}{1 + (b_{\min} \Lambda / R_d h' f_{\Lambda,d})^2}. \quad (\text{B13})$$

The effective Coulomb logarithm is found by averaging over all ψ :

$$\left\langle \frac{1}{2} \ln(1 + \Lambda^2)_{\text{eff}} \right\rangle = \frac{1}{4\pi} \int_0^{2\pi} \ln(1 + \Lambda^2)_{\text{eff}} d\psi. \quad (\text{B14})$$

This integral is solved numerically.

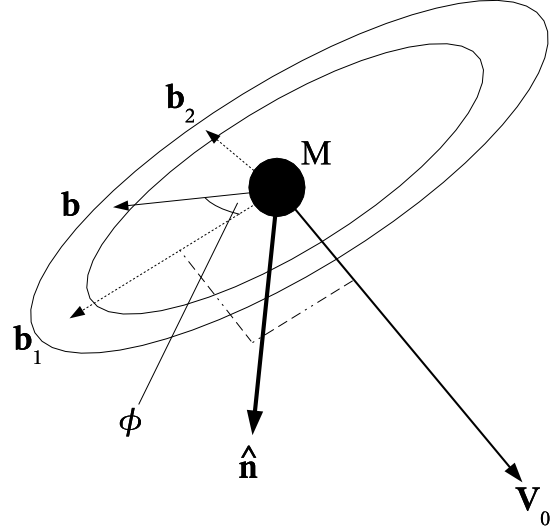


Figure B3. Geometry used in computing the rate of increase of velocity dispersion in direction $\hat{\mathbf{n}}$. Vectors \mathbf{b} , \mathbf{b}_1 and \mathbf{b}_2 lie in the plane of the annulus. Vector \mathbf{V}_0 is normal to the annulus and vector $\hat{\mathbf{n}}$ lies in the plane of \mathbf{V}_0 and \mathbf{b}_1 .

B3 Rate of Increase of Scattered Particle Velocity Dispersion

We now wish to determine the rate of increase of the one-dimensional velocity dispersion, measured in direction $\hat{\mathbf{n}}$, of the particles m due to dynamical friction scatterings. Since the centre of mass remains fixed during the scattering, $m\Delta\mathbf{V}_m + M\Delta\mathbf{V}_M = 0$. Therefore, to find the change in velocity of m we multiply the equations (7-10a) and (7-10b) of Binney & Tremaine by $-M/m$. Writing these in a more convenient form:

$$\Delta V_{m\perp} = -2V_0 \Lambda \frac{b}{b_{\max}} \left[1 + \Lambda^2 \frac{b^2}{b_{\max}^2} \right]^{-1}, \quad (\text{B15})$$

$$\Delta V_{m\parallel} = -2V_0 \left[1 + \Lambda^2 \frac{b^2}{b_{\max}^2} \right]^{-1}, \quad (\text{B16})$$

for the components of velocity perpendicular and parallel to the relative velocity vector \mathbf{V}_0 as measured in the frame in which the centre of mass of M and m is at rest.

Consider now the velocity of m in the frame in which the centre of mass of the central galaxy and its halo is at rest. The velocity changes are independent of frame so the final velocity of m in this frame is:

$$\mathbf{V}_m^{(f)} = \mathbf{V}_m + \frac{\mathbf{V}_0}{V_0} \Delta V_{m\parallel} + \frac{\mathbf{b}}{b} \Delta V_{m\perp}. \quad (\text{B17})$$

We are interested in the velocities in some direction $\hat{\mathbf{n}}$. The initial and final velocities of m in this direction are:

$$\mathbf{V}_{m,\hat{\mathbf{n}}}^{(i)} = \mathbf{V}_m \cdot \hat{\mathbf{n}}, \quad (\text{B18})$$

$$\mathbf{V}_{m,\hat{\mathbf{n}}}^{(f)} = \mathbf{V}_m \cdot \hat{\mathbf{n}} + \Delta V_{m\parallel} \cos \theta_{V_0} + \Delta V_{m\perp} \cos \theta_b, \quad (\text{B19})$$

where θ_{V_0} and θ_b are the angles between $\hat{\mathbf{n}}$ and \mathbf{V}_0 and $\hat{\mathbf{n}}$ and \mathbf{b} respectively. The change in the component of the kinetic energy in direction $\hat{\mathbf{n}}$ is therefore

$$\begin{aligned} \Delta E_{\hat{\mathbf{n}}} = & \frac{m}{2} \left\{ \Delta V_{m\parallel}^2 \cos^2 \theta_{V_0} + \Delta V_{m\perp}^2 \cos^2 \theta_b \right. \\ & + 2\Delta V_{m\parallel} \Delta V_{m\perp} \cos \theta_{V_0} \cos \theta_b \\ & \left. + 2\mathbf{V}_m \cdot \hat{\mathbf{n}} [\Delta V_{m\parallel} \cos \theta_{V_0} + \Delta V_{m\perp} \cos \theta_b] \right\} \quad (\text{B20}) \end{aligned}$$

To sum over all particles m , we first integrate around an annulus of constant $|\mathbf{b}|$. On this annulus, θ_{V_0} is constant and we can write the vector $\mathbf{b} = \mathbf{b}_1 \cos \phi + \mathbf{b}_2 \sin \phi$, where $\mathbf{b}_1 \cdot \mathbf{b}_2 = 0$, $|\mathbf{b}_1| = |\mathbf{b}_2| = b$ and ϕ is a parameter (see Fig. B3). We then note that

$$\begin{aligned} \int_0^{2\pi} \cos^2 \theta_b d\phi &= \int_0^{2\pi} \left[\frac{\mathbf{b}_1 \cdot \hat{\mathbf{n}}}{b} \right]^2 \cos^2 \phi \\ &+ \left[\frac{\mathbf{b}_2 \cdot \hat{\mathbf{n}}}{b} \right]^2 \sin^2 \phi \\ &+ 2 \left[\frac{(\mathbf{b}_1 \cdot \hat{\mathbf{n}})(\mathbf{b}_2 \cdot \hat{\mathbf{n}})}{b^2} \right] \sin \phi \cos \phi d\phi \\ &= \pi \left(\frac{\mathbf{b}_1 \cdot \hat{\mathbf{n}}}{b} \right)^2 + \pi \left(\frac{\mathbf{b}_2 \cdot \hat{\mathbf{n}}}{b} \right)^2. \quad (\text{B21}) \end{aligned}$$

If we choose \mathbf{b}_1 to be parallel to the projection of $\hat{\mathbf{n}}$ into the plane of the annulus then $\mathbf{b}_1 \cdot \hat{\mathbf{n}}/b = \sin \theta_{V_0}$ and $\mathbf{b}_2 \cdot \hat{\mathbf{n}}/b = 0$, so

$$\int_0^{2\pi} \cos^2 \theta_b d\phi = \pi \sin^2 \theta_{V_0}. \quad (\text{B22})$$

Using a similar approach, it is simple to show that $\int_0^{2\pi} \cos \theta_b d\phi = 0$. Thus, the change in energy becomes

$$\begin{aligned} \Delta E_{\hat{\mathbf{n}}} = & \frac{m}{2} \left\{ 2\pi \Delta V_{m\parallel}^2 \cos^2 \theta_{V_0} + \pi \Delta V_{m\perp}^2 \sin^2 \theta_{V_0} \right. \\ & \left. + 4\pi \mathbf{V}_m \cdot \hat{\mathbf{n}} \Delta V_{m\parallel} \cos \theta_{V_0} \right\}. \quad (\text{B23}) \end{aligned}$$

Substituting eqns. (B15) and (B16) we find

$$\begin{aligned} \Delta E_{\hat{\mathbf{n}}} = & \frac{mV_0^2}{2} \left\{ 8\pi \left[1 + \Lambda^2 \frac{b^2}{b_{\max}^2} \right]^{-2} \cos^2 \theta_{V_0} \right. \\ & + 4\pi \Lambda^2 \frac{b^2}{b_{\max}^2} \left[1 + \Lambda^2 \frac{b^2}{b_{\max}^2} \right]^{-2} \sin^2 \theta_{V_0} \\ & \left. - 8\pi \frac{\mathbf{V}_m \cdot \hat{\mathbf{n}}}{V_0} \left[1 + \Lambda^2 \frac{b^2}{b_{\max}^2} \right]^{-1} \cos \theta_{V_0} \right\}. \quad (\text{B24}) \end{aligned}$$

To find the total energy change we multiply by the flux of particles passing through the annulus, $nV_0 b db$, and integrate over b from 0 to b_{\max} . This gives

$$\begin{aligned} \frac{dE_{\hat{\mathbf{n}}}}{dt} = & \rho V_0^3 b_{\max}^2 \left\{ \frac{2\pi \cos^2 \theta_{V_0}}{1 + \Lambda^2} \right. \\ & + \pi \frac{(1 + \Lambda^2) \ln(1 + \Lambda^2) - \Lambda^2}{\Lambda^2(1 + \Lambda^2)} \sin^2 \theta_{V_0} \\ & \left. - 2\pi \frac{\mathbf{V}_m \cdot \hat{\mathbf{n}}}{V_0} \frac{\ln(1 + \Lambda^2)}{\Lambda^2} \cos \theta_{V_0} \right\}. \quad (\text{B25}) \end{aligned}$$

We next average over the velocity distribution of \mathbf{V}_m . The total rate of energy change is then

$$\begin{aligned} \frac{dE_{\hat{\mathbf{n}}}}{dt} = & \int \rho V_0^3 b_{\max}^2 \left\{ \frac{2\pi \cos^2 \theta_{V_0}}{1 + \Lambda^2} \right. \\ & + \pi \frac{(1 + \Lambda^2) \ln(1 + \Lambda^2) - \Lambda^2}{\Lambda^2(1 + \Lambda^2)} \sin^2 \theta_{V_0} \\ & \left. - 2\pi \frac{\mathbf{V}_m \cdot \hat{\mathbf{n}}}{V_0} \frac{\ln(1 + \Lambda^2)}{\Lambda^2} \cos \theta_{V_0} \right\} f(\mathbf{V}) d^3\mathbf{V}. \quad (\text{B26}) \end{aligned}$$

In general it seems that this equation is not analytically solvable, even if $f(\mathbf{V}_m)$ is an isotropic Gaussian. However, if we are interested in systems where random motions are much smaller than the bulk motion (such as galaxy disks), then we can approximate $f(\mathbf{V}_m) = \delta(\mathbf{V}_m - \mathbf{V}_d)$, where \mathbf{V}_d is the disk bulk velocity and δ is the Dirac delta function. Note that $\mathbf{V}_0 = \mathbf{V}_m - \mathbf{V}_M$ where \mathbf{V}_M is the velocity of M . For this case

$$\begin{aligned} \frac{dE_{\hat{\mathbf{n}}}}{dt} = & \rho V_0^3 b_{\max}^2 \left\{ \frac{2\pi \cos^2 \theta_{V_0}}{1 + \Lambda^2} \right. \\ & + \pi \frac{(1 + \Lambda^2) \ln(1 + \Lambda^2) - \Lambda^2}{\Lambda^2(1 + \Lambda^2)} (1 - \cos^2 \theta_{V_0}) \\ & \left. - 2\pi v_d \cos \theta_{v_d} \frac{\ln(1 + \Lambda^2)}{\Lambda^2} \cos \theta_{V_0} \right\}, \quad (\text{B27}) \end{aligned}$$

where $\cos \theta_{V_0} = v_d \cos \theta_{v_d} - v_M \cos \theta_{v_M}$. Here $v_d = V_d/V_0$ and θ_{v_d} is the angle between $\hat{\mathbf{n}}$ and \mathbf{V}_d , with similar definitions for v_M and θ_{v_M} . The efficiency of energy transfer to direction $\hat{\mathbf{n}}$ is then easily found by dividing the above by the same expression summed over three orthogonal directions (taking one of these to be parallel to \mathbf{V}_0 simplifies the summation):

$$\begin{aligned} \epsilon_{\hat{\mathbf{n}}} = & \left\{ \frac{2 \cos^2 \theta_{V_0}}{1 + \Lambda^2} + \frac{(1 + \Lambda^2) \ln(1 + \Lambda^2) - \Lambda^2}{\Lambda^2(1 + \Lambda^2)} (1 - \cos^2 \theta_{V_0}) \right. \\ & \left. - 2v_d \cos \theta_{v_d} \frac{\ln(1 + \Lambda^2)}{\Lambda^2} \cos \theta_{V_0} \right\} / \left\{ \frac{2}{1 + \Lambda^2} \right. \\ & + 2 \frac{(1 + \Lambda^2) \ln(1 + \Lambda^2) - \Lambda^2}{\Lambda^2(1 + \Lambda^2)} \\ & \left. - 2v_d \cos \theta_{v_d} \frac{\ln(1 + \Lambda^2)}{\Lambda^2} \right\}. \quad (\text{B28}) \end{aligned}$$

We are interested specifically in the vertical velocity dispersion of a galactic disk. In this case \mathbf{V}_d lies in the disk plane, while $\hat{\mathbf{n}}$ is perpendicular to that plane. Consequently $\cos \theta_{v_d} = 0$ and the above expression simplifies to

$$\begin{aligned} \epsilon_z = & \left\{ \frac{2 \cos^2 \theta_{V_0}}{1 + \Lambda^2} + \frac{(1 + \Lambda^2) \ln(1 + \Lambda^2) - \Lambda^2}{\Lambda^2(1 + \Lambda^2)} (1 - \cos^2 \theta_{V_0}) \right\} \\ & / \left\{ \frac{2}{1 + \Lambda^2} + 2 \frac{(1 + \Lambda^2) \ln(1 + \Lambda^2) - \Lambda^2}{\Lambda^2(1 + \Lambda^2)} \right\}. \quad (\text{B29}) \end{aligned}$$

This expression is then used in eqn. (2) to calculate the vertical heating rate of galaxy disks. Note that $0 \leq \epsilon_z \leq 1$, as expected for an efficiency factor.

APPENDIX C: DISK SURFACE ENERGY DENSITIES

We here derive expressions for the different contributions to the surface energy density of the disk. These are used in §2.2.2.

We assume a disk with a density structure

$$\rho_d(R, z) = \Sigma(R) \frac{\text{sech}^2(z/H_d)}{2H_d}. \quad (\text{C1})$$

with H_d constant with radius. Assuming that the disk is thin, $H_d \ll R$, the potential of the disk can be found by approximating the density distribution as a set of infinite, homogeneous planes, such that

$$\begin{aligned} \phi_d(R, z) &= \int_{-\infty}^{\infty} 2\pi G \rho_d(R, z) |z - z'| dz' + \phi_d(R, 0) \\ &= 2\pi G \Sigma(R) H_d [\ln \cosh(z/H_d) + \ln 2] + \phi_d(R, 0) \end{aligned} \quad (\text{C2})$$

Close to the disk plane, the z -component of the force due to the spherical halo plus bulge is

$$F_h = -\frac{GM_h(R)}{R^3} z, \quad (\text{C3})$$

hence the potential due to these components is

$$\begin{aligned} \phi_h(R, z) &\approx \int_0^z \frac{GM_h(R)}{R^3} z' dz' + \phi_h(R, 0) \\ &= \frac{GM_h(R)}{2R^3} z^2 + \phi_h(R, 0). \end{aligned} \quad (\text{C4})$$

Referencing all energies to $z = 0$, we can neglect the final terms in the above equations. We can now calculate the different contributions to the disk vertical energy per unit area, where necessary using the thin disk approximation $H_d \ll R$. The gravitational self-energy of the disk is then

$$\begin{aligned} w_{dd}(R) &= \frac{1}{2} \int_{-\infty}^{\infty} \phi_d(R, z) \rho_d(R, z) dz \\ &= \pi G \Sigma(R)^2 H_d. \end{aligned} \quad (\text{C5})$$

The disk-halo gravitational potential energy is

$$\begin{aligned} w_{dh}(R) &= \int_{-\infty}^{\infty} \phi_h(R, z) \rho_d(R, z) dz \\ &= \frac{\pi^2}{24} \frac{GM_h(R)}{R^3} \Sigma_d(R) H_d^2, \end{aligned} \quad (\text{C6})$$

and the kinetic energy of the disk is

$$t_z(R) = \frac{1}{2} \Sigma(R) \sigma_z^2(R). \quad (\text{C7})$$

APPENDIX D: CONVERGENCE TESTS ON N-BODY SIMULATIONS

We repeated all the simulations of models G1S1 to G1S15 with one half and one quarter the number of particles, labelling these runs G1S1^{1/2}, G1S1^{1/4} etc. (In each case, we scaled the softening in proportion to the mean interparticle separation.) Figures D1 and D2 compare the results for two representative models (G1S1 and G1S5) run with different

numbers of particles. In both cases, the position and velocity of the satellite are well converged up until the very final stages of the satellite's life (at which point it becomes difficult to measure these quantities accurately from the simulation anyway). The higher resolution simulations lose mass from the satellite somewhat more rapidly at late times, but the differences are minor and the mass loss rate is well determined by the simulations.

The convergence behaviour seems poorer for the change in vertical kinetic energy ΔT_z (in which the energy of the unperturbed disk from model G1S0 has been subtracted off). For the model G1S5, the difference in the final ΔT_z of $(0.02 - 0.03) \times 10^{14} M_\odot \text{km}^2 \text{s}^{-2}$ between the highest and lowest resolution runs could result mostly from the error in the energy of the unperturbed disk that is subtracted off, since the variation in this value between different realizations is around $(0.02 - 0.03) \times 10^{14} M_\odot \text{km}^2 \text{s}^{-2}$ in the low resolution case. However, for model G1S1 the differences in ΔT_z between the high and low resolution runs are much bigger than can be explained by errors in the subtraction of the unperturbed disk contribution. In this case, the behaviour of ΔT_z is not even monotonic as the number of particles is increased. We have investigated this further by repeating some of the lowest resolution simulations using a different sequence of random numbers in generating the initial conditions. We find that this leads to significant variations in ΔT_z , comparable to those seen between the lowest resolution and higher resolution simulations. It therefore seems that the amount of disk heating by satellites is sensitive to stochastic variations in the initial conditions, over and above the two-body relaxation which heats the unperturbed disk. Comparing the highest and lowest resolution runs, we find that the error in the low-resolution estimate of ΔT_z is $\sim 30\%$ for model G1S5, but $\sim 100\%$ for model G1S1. The convergence of ΔT_z with increasing particle number thus seems to depend on the orbital properties of the satellite, with different numbers of particles being required to achieve the same degree of convergence in different cases. A more comprehensive study of convergence in a variety of models will be required to address this question fully.

APPENDIX E: ORDER OF MAGNITUDE ESTIMATES OF DISK THICKNESSES

In this appendix we make order of magnitude estimates for the thicknesses of disks resulting from heating by satellites and by stars scattering from giant molecular clouds.

E1 Heating by Satellites

We assume a distribution of satellite halo masses $dN/dM = AM^{-1.7}$, where A is a constant, with a maximum mass of $f_{\text{max}} = 0.01$ of the total halo mass and making up a fraction $f_{\text{mass}} = 0.1$ of the total halo mass (consistent with numerical simulations; Springel et al. 2001). Then,

$$A = 0.3 f_{\text{mass}} M_{\text{halo}}^{0.7} / f_{\text{max}}^{0.3}. \quad (\text{E1})$$

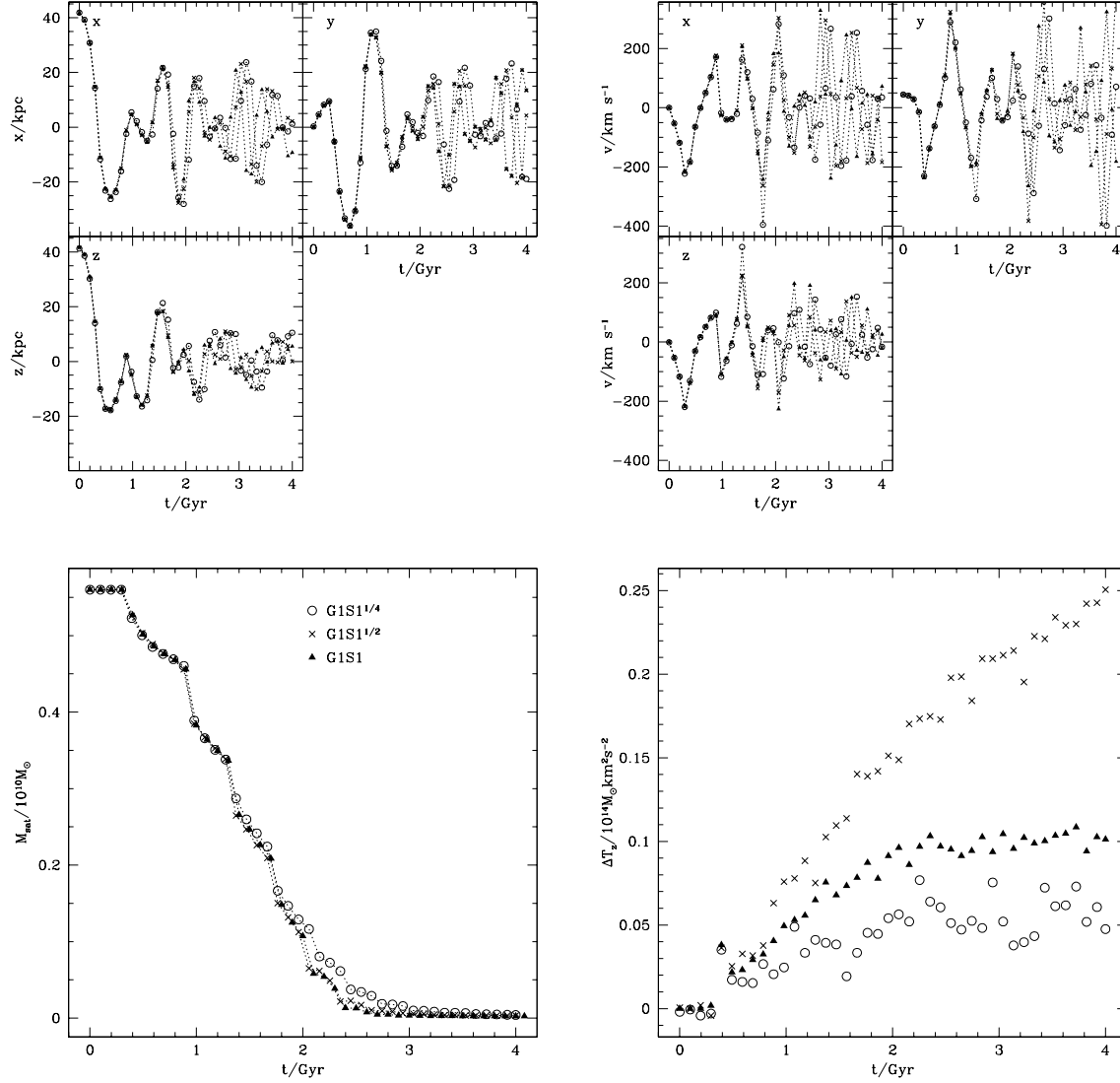


Figure D1. Convergence tests for model G1S1. Results are shown for the standard simulation (circles), model G1S1^{1/2} (which has half the number of particles of G1S1; crosses) and model G1S1^{1/4} (which has one quarter the number of particles of G1S1; triangles). Points are connected by dotted lines to guide the eye only—lines are not intended as a realistic interpolation of the points. *Top left-hand panel:* The orbital position of the satellite as a function of time. *Top right-hand panel:* The orbital velocity of the satellite as a function of time. *Lower left-hand panel:* The remaining bound mass of the satellite as a function of time. *Lower right-hand panel:* The change in the vertical component of the disk kinetic energy due to heating by the satellite as a function of time.

Taking the Chandrasekhar formula for dynamical friction (eqn. B6), the power deposited by a satellite is, to order of magnitude

$$P = 4\pi \frac{G^2 M_s^2}{V_s} \ln \Lambda \rho_d. \quad (\text{E2})$$

Assuming that heating is effective primarily within one scale height of the disk, then heating occurs over a fraction of roughly $H_d/2\pi r_{\text{orb}}$ of the satellite's orbit, where r_{orb} is the orbital radius. Allowing for an efficiency of vertical heating ϵ_z and integrating over masses, the total energy transfer in

time t is given by

$$\begin{aligned} E &= 2t \frac{G^2}{V_s} \ln \Lambda \frac{M_d}{4\pi R_d^3 h} \epsilon_z \frac{R_d h}{r_{\text{orb}}} \int_0^{f_{\text{max}} M_{\text{halo}}} A M_s^{-1.7} M_s^2 dM_s \\ &= 2 \frac{G^2}{V_s} \ln \Lambda \frac{M_d}{4\pi R_d^3 h} \epsilon_z \frac{R_d h}{r_{\text{orb}}} 0.3 f_{\text{mass}} M_{\text{halo}}^2 f_{\text{max}}. \end{aligned} \quad (\text{E3})$$

Equating to the energy of the disk, as given by eqn. (8) after ignoring the contribution proportional to h^2 as this is typically small, and solving for h

$$h = \frac{8}{3\pi} 0.3 f_{\text{mass}} f_{\text{max}} \epsilon_z \frac{G M_{\text{halo}}^2 \ln \Lambda}{V_s R_d r_{\text{orb}} M_d} t, \quad (\text{E4})$$

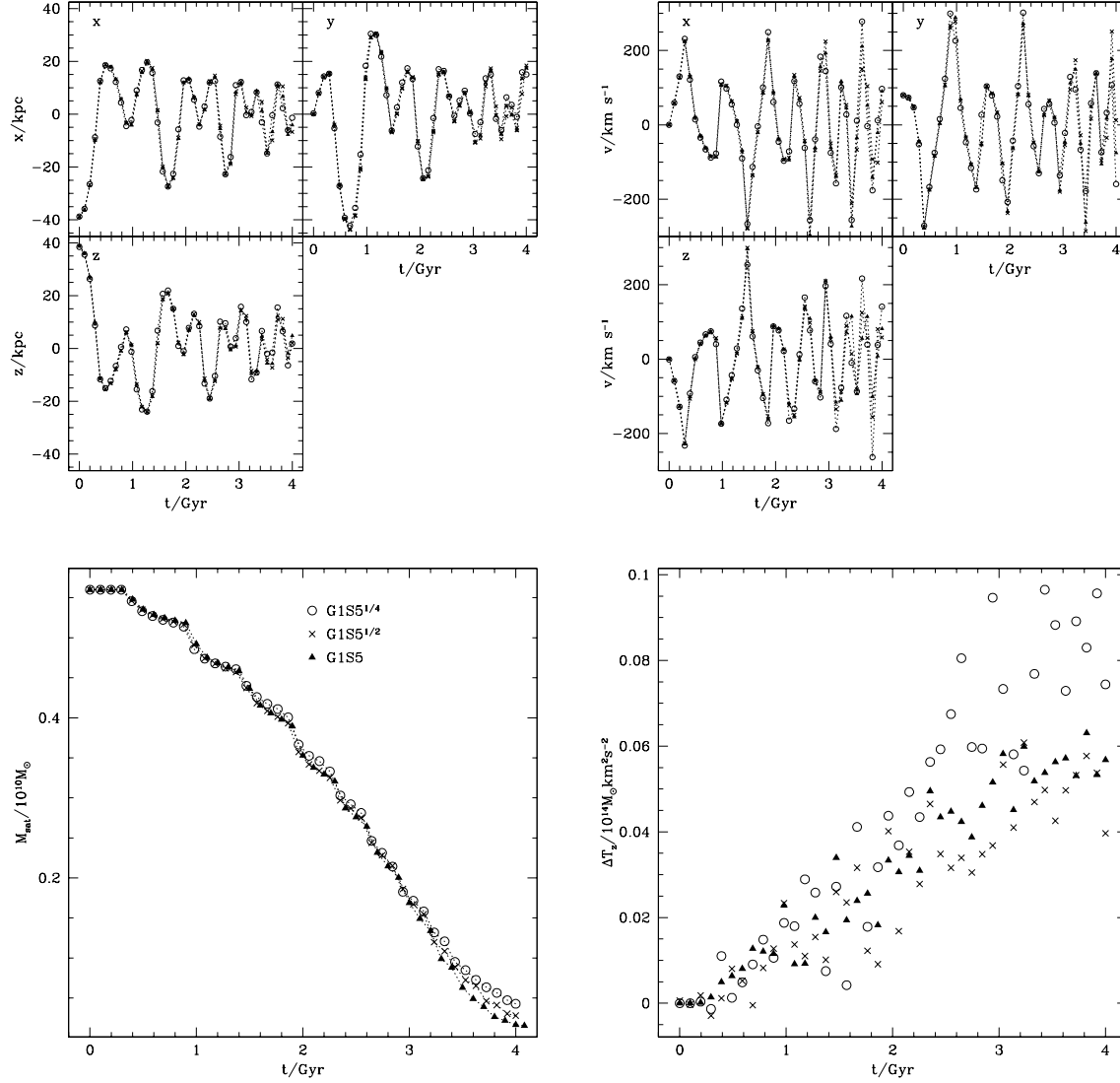


Figure D2. Convergence tests for model G1S5. Results are shown for the standard simulation (circles), model G1S5^{1/2} (which has half the number of particles of G1S5; crosses) and model G1S5^{1/4} (which has one quarter the number of particles of G1S5; triangles). The different panels are as for Figure D1.

or

$$\begin{aligned}
 h &= 0.16 \left(\frac{f_{\text{mass}}}{0.1} \right) \left(\frac{f_{\text{max}}}{0.01} \right) \left(\frac{\epsilon_z}{0.3} \right) \left(\frac{M_{\text{halo}}}{10^{12} M_{\odot}} \right)^2 \left(\frac{\ln \Lambda}{3} \right) \\
 &\times \left(\frac{V_s}{200 \text{ km/s}} \right)^{-1} \left(\frac{R_d}{3.5 \text{ kpc}} \right)^{-1} \left(\frac{r_{\text{orb}}}{200 \text{ kpc}} \right)^{-1} \\
 &\times \left(\frac{M_d}{5 \times 10^{10} M_{\odot}} \right)^{-1} \left(\frac{t}{\text{Gyr}} \right). \quad (\text{E5})
 \end{aligned}$$

E2 Heating by Scatterings from Giant Molecular Clouds

We begin with eq. (10), which we approximate to order of magnitude (replacing $d\epsilon_z/dt$ with ϵ_z/t etc.) as

$$E = 2 \frac{G^2 M_d M_c \Sigma_c}{\sigma_z^2} \nu \ln \Lambda_c \alpha_s^3(\beta) K_s(\beta) t. \quad (\text{E6})$$

Inserting eqn. (7) to eliminate σ_z (we again ignore the contribution proportional to h^2) this reduces to

$$E = \frac{2}{\pi} \frac{G M_d M_c}{R_d h} \frac{\Sigma_c}{\Sigma_d} \ln \Lambda_c \nu \alpha_s^3(\beta) K_s(\beta) t. \quad (\text{E7})$$

Equating to the energy of the disk and solving for h results in

$$h^2 = \frac{32}{3\pi} \frac{M_c}{M_d} f \ln \Lambda_c \nu \alpha_s^3(\beta) K_s(\beta) t, \quad (\text{E8})$$

where $f = \Sigma_c/\Sigma_d$. This can be expressed as

$$h = 7.2 \times 10^{-3} \left[\frac{f}{0.025} \right]^{1/2} \left[\frac{M_c/M_d}{3 \times 10^{-5}} \right]^{1/2} \left[\frac{\ln \Lambda}{3} \right]^{1/2}$$

$$\times \left[\frac{\nu}{90 \text{ Gyr}^{-1}} \right]^{1/2} \left[\frac{\alpha_S(\beta)}{0.7} \right]^{3/2} \left[\frac{K_S(\beta)}{0.15} \right]^{1/2} \left[\frac{t}{\text{Gyr}} \right]^{1/2} \quad (\text{E9})$$